March 2015
Volume 121
Issue 1947
£5.20

www.electronicsworld.co.uk

Electronics WORLD

THE ESSENTIAL ELECTRONICS ENGINEERING MAGAZINE

Powering Smart Wearable Devices

By Linear Technology

ALSO IN THIS ISSUE:

- Embedded design
- LDOs
- Filters

Technology
Researchers fight spying practices with technology

Special Report:
Analog design

Products
Latest controllers and other ICs

TELEDYNE LECROY
Everywhereyoulook™

Complete Power Analysis for 3 Phase Motor Drives

NEW! Motor Drive Analyzer MDA800 – 8 Channel, 12-bit, up to 1 GHz

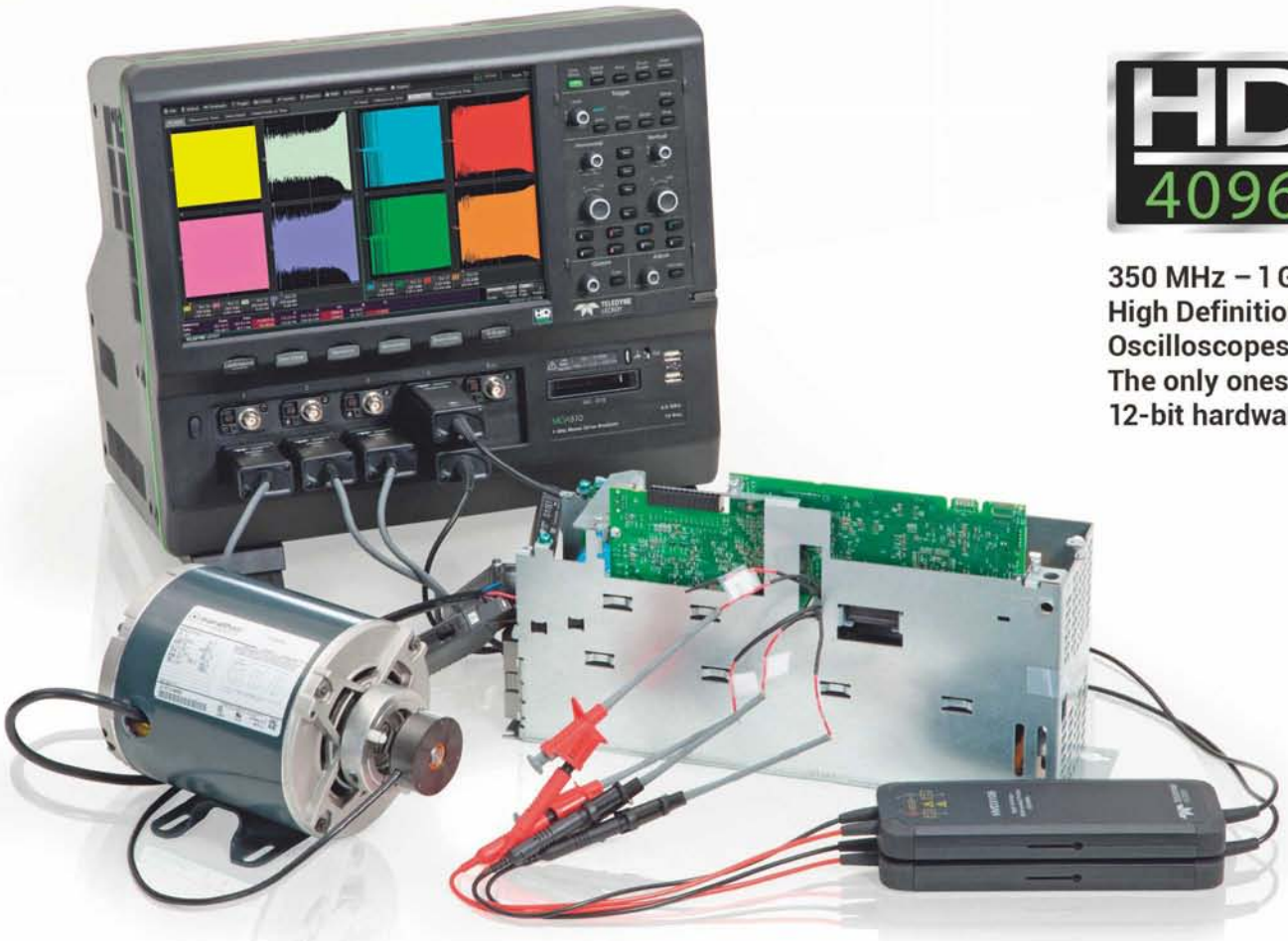

HD 4096

350 MHz – 1 GHz High Definition Oscilloscopes – The only ones with 12-bit hardware

Who's**doing**that?

teledynelecroy.com

Cover supplied by LINEAR TECHNOLOGY
More on pages 16-17

REGULARS

FEATURES

THE FUTURE OF THE WEARABLES MARKET

> Juniper Research's report predicts fitness wearables will almost treble in use by 2018, compared to an estimated 19 million in-use devices in 2014

Wearable, printed, biosensors startup company Electrozyme claims that despite great innovation in wearable devices, consumer interest remains low.

"Innovation is stagnating in the wearable devices domain. New wearable devices emerge on a daily basis, nearly all of which feature the same sensing capabilities – heart rate, motion, skin conductivity and the like. It is for this reason that one of the unspoken maladies in the wearable technology field is the lack of customer engagement several months following their wearable device purchase. In essence, such devices are thrown into the sock drawer following periods of inactivity never to be used again. This fate would never confront a user's smartphone," said Joshua Windmiller, Electrozyme co-founder and CEO.

Windmiller, however, expects that new sensor technologies, such as printed electronics, will be the deciding factor for the success of wearables.

"Printed electronics will serve as an enabling technology that will fuel the development of the next generation wearable devices and allow product developers to realize wearable designs that have widespread appeal."

Electrozyme develops sensors for the sports, fitness, wellness and healthcare sectors, and among its novel devices are a skin-applied biosensor for metabolite and electrolyte quantification, and a scavenging epidermal biofuel cell that draws power from perspiration.

"Particular emphasis will be on low-cost, high-throughput methods leveraged to fabricate such devices, as well as the challenges that confront the emergent field of epidermal biosensors going forward," said Windmiller.

According to a new report by market analysis firm Juniper Research, fitness wearables will almost treble in use by 2018, from an estimated 19 million in-use devices in 2014. Juniper expects fitness to remain the dominant wearables segment until then, driven mainly by lower retail prices.

Juniper's report, *"Smart Health & Fitness Wearables: Device Strategies, Trends & Forecasts 2014-2019"*, states that wearable fitness devices will split into two categories: basic trackers, like the $13 Xiaomi MiBand, and more complex devices, such as the Fitbit Surge, Microsoft Band and Samsung Gear Fit, which in addition to fitness features also offer various notifications and music control. Juniper also predicts that, in addition to standalone devices and smartphones, increasingly capable smart watches will incorporate multiple sensors, eliminating the need for separate devices to measure health and fitness biometrics.

The same report anticipates that sales of healthcare-focused wearable devices will increase, from wearable ECGs (electrocardiograms) to glucose monitors and insulin pumps. While they are currently used where self-medication is the norm, capabilities will expand to allow monitoring by healthcare professionals in other locations.

Juniper's report concludes that consumer engagement is a key pain-point for fitness wearables, but that some companies are figuring out business models around these devices to counteract the consumer malaise. One such company, GOQii, is pioneering a new service-based business model, offering contact with fitness coaches via their device. The market analysis firm writes that with technological barriers coming down, larger players in the market are moving beyond devices to produce operating systems and databanks to manage the information generated by wearables. Recent examples include Google's Android Wear, Qualcomm's 2net and Samsung's Digital Health Initiative.

Aging populations and increased chronic-disease incidence are expected to continue to drive healthcare strategies, with the medical profession increasingly relying on digital health. This will manifest itself in several ways including: healthcare companies investing in major digital healthcare players such as Epocrates and AirStrip; advanced EHR (Electronic Health Records) becoming the 'glue' to create wider digital health ecosystems; and regulatory authorities embracing digital health and imposing less stringent regulatory obligations on digital health companies.

Juniper's report can be found on line at www.juniperresearch.com

EDITOR: Svetlana Josifovska
Tel: +44 (0)1732 883392
Email: svetlanaj@sjpbusinessmedia.com

SALES: Sunny Nehru
Tel: +44 (0)20 7933 8974
Email: sunnyn@sjpbusinessmedia.com

DESIGN: Tania King
PUBLISHER: Justyn Gidley

ISSN: 1365-4675

PRINTER: Buxton Press Ltd

SUBSCRIPTIONS:
Subscription rates:
1 year: £62 (UK);
£89 (worldwide)
Tel/Fax +44 (0)1635 879361/868594
Email: electronicsworld@circdata.com

SJP business media

2nd Floor,
52-54 Gracechurch Street,
London, EC3A 0EH

Follow us on Twitter
@electrowo

Join us on LinkedIn

RESEARCHERS TACKLE NEW CLASS OF HACKERS

There has been a new generation of hackers who analyze low-power electronic signals emitted from a laptop or mobile phone, even when the devices are not connected to the Internet or Wi-Fi. The hacking could take place anywhere, even in places such as coffee shops.

Researchers at the Georgia Institute of Technology are now investigating where information leaks (known as side-channel signals) originate, so they can help engineers develop prevention strategies.

"People are focused on security for the Internet and on wireless communications, but we are concerned with what can be learned from a computer without it intentionally sending anything," said Alenka Zajic, an assistant professor in Georgia Tech's School of Electrical and Computer Engineering.

The research showed that information such as passwords can be obtained from switched off devices, and even through walls. Side-channel emissions can be measured several feet away from an operating computer using a variety of eavesdropping methods. Electromagnetic emissions can be received using nearby antennas. Acoustic emissions – sounds produced by electronic components such as capacitors – can be picked up by microphones, and voltage regulators produce emissions that can carry signals produced elsewhere in the laptop. Information on power fluctuations, which can help hackers determine what a computer is doing, can be measured by fake battery chargers plugged into power outlets adjacent to a laptop's power converter. Some signals can be picked up by a simple AM/FM radio, while others require more sophisticated spectrum analyzers.

Georgia Tech researchers Alenka Zajic and Milos Prvulovic use a simple AM/FM radio to pick up side-channel signals from a cell phone
(Credit: Rob Felt)

"We are identifying the parts of the devices that leak the most. That information can guide efforts to redesign them, and on an architectural level, perhaps change the instructions in the software to change the device behaviour," said Zajic.

Each computer operation has a different potential for leaking information. The microprocessor draws different amounts of current depending on the operation, creating fluctuations that can be measured. Saving data to memory also requires a large amount of current, creating a "loud" operation. Quieting such operations will make hacking more difficult.

The researchers are also now studying smartphones, whose compact design and large differential between idle and in-use power may make them more vulnerable.

ZHAGA CONSORTIUM PREPARES NEW SPECIFICATION FOR COB LED ARRAYS

The Zhaga Consortium, which develops specifications for interchangeable LED light sources, is now working on a new Zhaga Book to include Chip-on-Board (COB) LED arrays.

COB arrays are already in widespread use throughout the LED lighting industry, but different manufacturers offer a wide range of alternative sizes. This creates problems for luminaire makers and other stakeholders, such as COB holder suppliers, and limits their options to use alternative products from different suppliers without changing their luminaire or holder designs.

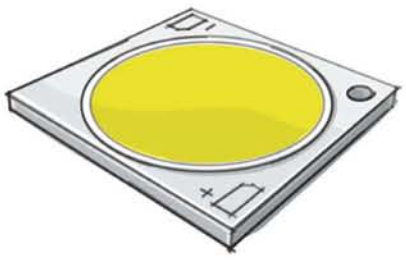

The Zhaga Consortium is hard at work defining the new COB LED arrays specifications

"We consulted many luminaire makers and received broad support for our plans to standardize this type of LED light source," said Musa Unmehopa, Secretary General of the Zhaga Consortium. "These companies asked us to standardize properties such as the mechanical dimensions of the module, the position of electrodes and the diameter of the light-emitting surface."

Zhaga standardization removes arbitrary variations in a small number of parameters, in order to enable interchangability of LED light sources, simplifying the comparison and selection of products for customers. COB-array makers can now focus on areas with value-added differentiation, such as thermal properties, quality of light or luminous efficacy.

"For the Zhaga Books to be successful, they need to reflect the wishes of the market," said Unmehopa. "We welcome any input from COB makers or other companies, who are invited to join Zhaga and contribute to the ongoing discussions."

LED MODULES SPECIFICATION DETAILS

The new Zhaga Book will define LED light engines comprising rectangular and square LED modules with a circular light-emitting surface (LES) and a separate LED driver. The Book will define a family of modules with different dimensions.

In the majority of cases, modules that are compliant with the new Book will employ COB technology, in which the LED chips are mounted directly onto a PCB, for the light-emitting section. However, the Zhaga specification will not prevent the use of alternative approaches.

The Consortium has decided to specify a family of six rectangular or square modules, with the following PCB dimensions: 12 x 15 mm, 16 x 19 mm, 19 x 19 mm, 20 x 24 mm, 24 x 24mm and 28 x 28 mm.

In common with other Zhaga specifications, the new Book will only restrict the parameters necessary to enable interchangeability, which include PCB dimensions and thickness, location of the LES centre point, the position and size of the electrodes, and the location of thermal measurement points. Screw holes will be optional, since many COB arrays are mounted directly using thermal interface material.

Adding Connectivity to Your Design

Bluetooth® | MiWi™ | USB | Wi-Fi CERTIFIED

ZigBee® Control your world | Ethernet | CAN | LIN

Microchip offers support for a variety of wired and wireless communication protocols, including peripheral devices and solutions that are integrated with a PIC® Microcontroller (MCU).

Wireless connectivity options include: Wi-Fi®, Bluetooth®, 802.15.4/ ZigBee® and out proprietary MiWi™ wireless networking protocol. Other connectivity protocols supported include USB (device, host, OTG and hubs), Ethernet, CAN, LIN, IrDA® and RS-485.

All of these protocols are supported with free software libraries, low-cost development platforms and free samples.

microchip DIRECT
www.microchipdirect.com

MICROCHIP

microchip.com/connectivity

THIS SERIES PRESENTS THE RASPBERRY PI SINGLE-BOARD COMPUTER, ITS FEATURES AND BENEFITS, AND HOW TO USE IT IN VARIOUS PROJECTS

Installing The Raspberry Pi Software

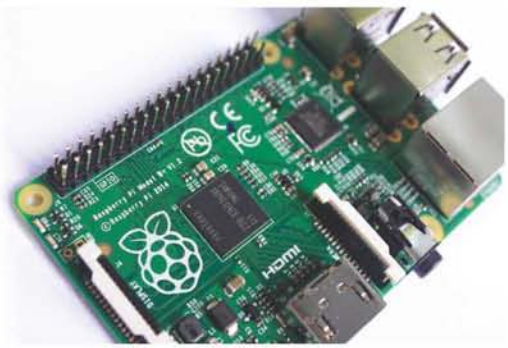

BY **GARETH HALFACREE**

Once you know the name of the package you want to install, switch to the apt-get command to install it.

Installing software is a privilege afforded only to the root user, since it affects all users of the Raspberry Pi. As a result, the commands will need to be prefaced with sudo to tell the operating system that it should be run as the root user.

For example, to install the package nethack-console (a console-based, randomly-generated, role-playing game), simply use the install command with apt-get as follows: sudo apt-get install nethack-console.

Some packages rely on other packages. A programming language may depend on a compiler, a game engine on graphics files, or an audio player on codecs for playing back different formats, known in Linux terms as dependencies.

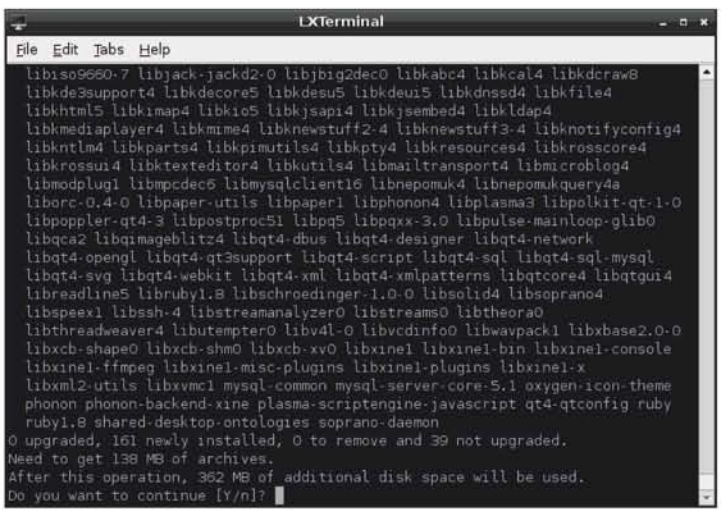

Figure 1: Apt listing the dependencies for the open office.org package

Dependencies are one of the biggest reasons for using a package manager like apt rather than installing software manually. If a package depends on other packages, apt will automatically find them (see Figure 1) and prepare them for installation. If this happens, there will be a prompt asking whether you want to continue. If you do, type the letter Y and press Enter.

Uninstalling Software

If you decide you no longer want a piece of software, apt-get also includes a remove command that cleanly uninstalls the package, along with any dependencies that are no longer required. When using a smaller SD card with the Pi, the ability to try out software and quickly remove it is very useful. To remove nethack-console, simply open the terminal and type the command: sudo apt-get remove nethack-console.

The remove command has a more powerful brother in the form of the purge command. Like remove, the purge command gets rid of software that's no longer required. Where remove leaves the software's configuration files intact, purge removes everything. If you've got yourself into a mess customising a particular package that no longer works, purge is the command to use. For example, to purge nethack-console, you would just type: sudo apt-get purge nethack-console.

Upgrading Software

In addition to installing and uninstalling packages, apt can be used to keep them up to date.

Upgrading a package through apt ensures that you've received the latest updates, bug fixes and security patches.

Before trying to upgrade a package, make sure the apt

cache is as fresh as possible by running an update: sudo apt-get update.

When upgrading software, you have two choices: upgrade everything on the system at once or upgrade individual programs. If you just want to keep your entire distribution updated, the former is achieved by typing: sudo apt-get upgrade.

To upgrade an individual package, simply tell apt to install it again. For example, to install a nethack-console upgrade, type: sudo apt-get install nethack-console.

If the package is already installed, apt will treat it as an in-place upgrade. If you're already running the latest version available, apt will simply tell you it cannot upgrade the software and then exit. ●

This is an edited extract from the Raspberry Pi User Guide, 3rd edition, by Eben Upton and Gareth Halfacree

RASPBERRY PI USER GUIDE

Gareth Halfacree is a co-author of the Raspberry Pi User Guide alongside project co-founder Eben Upton.

Halfacree often reviews, documents and contributes to projects such as GNU/Linux, LibreOffice, Fritzing and Arduino. He is also the creator of the Sleepduino and Burnduino open-hardware projects, which extend the capabilities of the Arduino electronics-prototyping system.

We have copies of the Raspberry Pi User Guide to give away at the end of the series. Register your interest by writing to the Editor at svetlanaj@sjpbusinessmedia.com, mentioning the title of the book in the heading.

Managing Graphic Resources

LUCIO DI JASIO, ELECTRONICS ENGINEER AND TECHNICAL AUTHOR, PRESENTS THIS SERIES ON EMBEDDED USER INTERFACE DESIGN ON A BUDGET

As little as TFT displays cost today, once we spend the money we might feel obliged to use every single pixel and every single colour achievable. Unfortunately there are problems with this approach. The main problem is perhaps more general; when it comes to user interfaces, more is *not* always better.

Using colour judiciously can greatly enhance the visual impact of the user interface. Use too much colour or without consistency, and the effect is the exact opposite. When too many pieces of information on a screen full of data are vying for your attention, using colour and/or too much contrast leads to loss of focus and usability.

A similar case can be built for "density" of data/figures on the screen. Nothing sharpens user attention on an item better than empty space around it.

The theory has been studied for decades, and perhaps the most convincing demonstration is from web design practices. Compare the graceful and almost understated look and feel of a web site such as Apple's, Google's or media companies' to the psychedelic look and feel of the most popular web sites of the early days. The point is that, while the hard specs of a display (size, resolution, colour palette, size, etc) matter, the way they are used matters even more. This brings us to the all-important subject of "graphic resources", which is a fancy way of referring to the textual and pictorial elements of the user interface design.

Managing Tight Budgets

The effects of RAM and Flash memory space limitations that characterize every embedded application are even more acute in graphical user interfaces. A few back-of-the-envelope calculations quickly reveal the magnitude of the problem when we consider a basic "image" visual element.

On a humble Mikromedia board with a "small" TFT display capable of 320 x 240 pixels with 16-bit colour, the largest object that can be represented (think of a background image) requires (320 x 240 x 2) 150kbytes of memory. That is much more RAM than any available microcontroller (PIC24F, PIC24EP, PIC32MX) can offer. Even assuming the image is retrieved directly from Flash memory, that can constitute a significantly large portion of the of the total program memory available on a microcontroller. Using judiciously smaller graphical elements and making use of compression methods is therefore an absolute requirement, but it might not be enough.

Mikromedia boards offer some hardware assistance to relieve pressure on the memory budget in two ways: providing additional Flash memory (1 Megabyte) in the form of a serial flash device (see Figure 1) and by means of a micro-SD-card media interface (several Gigabytes of additional storage); see Figure 2.

Both options expand the amount of storage space available to an application, but it is important to notice that in both cases a tradeoff is made between space and time required to retrieve the data. Also, interestingly, in both cases the SPI port is used to access the external memory devices. Two separate modules of the Microchip Library of Applications (MLA) library (the MDD File System and the Serial Flash Board Support Package) can help abstract the specific interface details and make the resources available to the graphics library.

Bitmaps

To understand better the performance side of the equation, we need to dig deeper in the way images (for now) can be stored in a given type of media. The most straightforward way is a table, also known as a bitmap. Each pixel in a given bitmap can be represented using a minimum of 1 bit, which would produce a monochromatic image (on or off, black or white); 4-bit providing up to 16 colours (appropriately chosen from a palette); 8-bit providing 256 colours (once more from a palette); or in full colour resolution when every pixel is given the full choice of all colours the display can do. The size in memory of the resulting bitmap resource changes dramatically.

As mentioned earlier, we must understand how different images (icons, pictures, etc) can be represented to achieve the required user interface impact while incurring minimum memory cost.

The MLA graphics library supports all the above options and,

Figure 1: Mikromedia board, serial Flash (M25P80) interface

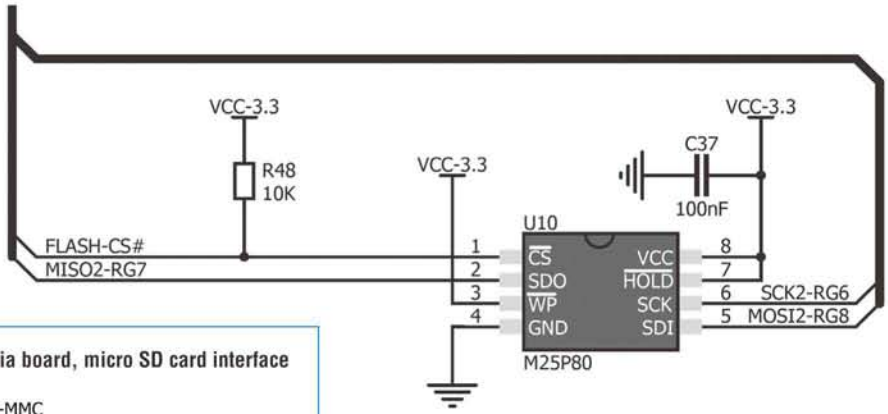

Figure 2: Mikromedia board, micro SD card interface

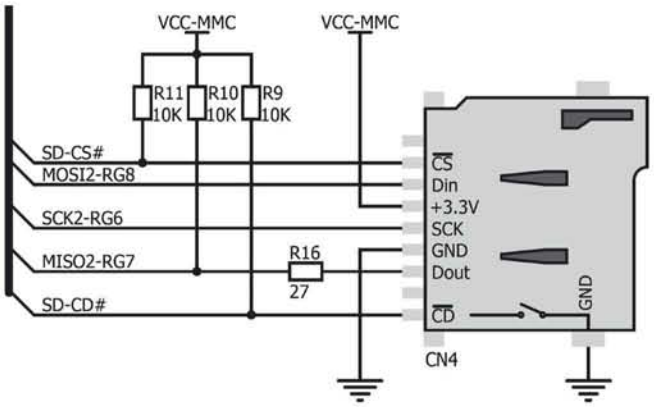

most importantly, comes with an additional tool – the Graphic Resource Converter (GRC) – to help convert images between formats and to pack them up for arrangement in the microcontroller's Flash memory.

Fonts

When we focus on the textual elements of a user interface, we quickly discover that the problems are exactly the same as with the more general case of images. In effect fonts are large collections of smaller images (glyphs), and although we don't worry so much about mixing and matching colours, once we consider the use of multiple font sizes, or large character sets when supporting Asian languages within our applications, they can add up to very large memory requirements.

Once more, the MLA Graphic Resource Converter tool can help manage the resources, by scaling and pre-rendering fonts and even selectively filtering out a few characters/symbols for maximum efficiency.

The Graphic Configuration File Returns

The MLA graphics library allows the mixing and matching of images and fonts that might be stored in RAM, internal Flash and/or external (serial) Flash for use in the application, provided care is taken to appropriately set up a few configuration parameters. Normally this takes place in the GraphicConfig.h file (see last month's column).

```
...
#define USE_FONT_FLASH                  // Support fonts located in internal flash
//#define USE_FONT_EXTERNAL             // Support fonts located in external memory

/*********************************************************************
* Overview: Similar to Font data bitmaps can also be placed in
*           two locations. One is in FLASH memory and the other is
*           from external memory.
*           Defining one or both enables the support for bitmaps located
*           in internal flash and external memory.
*           - USE_BITMAP_FLASH - Font in internal flash memory support.
*           - USE_BITMAP_EXTERNAL - Font in external memory support.
*
*********************************************************************/
#define USE_BITMAP_FLASH                // Support bitmaps located in internal flash
#define USE_BITMAP_EXTERNAL             // Support bitmaps located in external memory
...
```

Figure 3: Segment of the GraphicConfig.h

Compression And File Formats

However, there are cases when all the care taken to use the smallest possible bitmaps and fonts is not enough. Then, we can use compression, trading some more microcontroller performance for more space and resources. Bitmaps can be compressed using lossless algorithms such as RLE and GIF, or lossy compression mechanisms, such as the popular JPG format. The level of compression achievable is heavily dependent on the type of data at hand and the amount of performance we are willing to trade.

Synthetic images, such as icons, and basic graphical elements can be best compressed using RLE or GIF, while photographic images are best compressed using JPG. Note that while RLE requires relatively small amounts of computational power and can be used even for font resources, GIF and JPG in particular can be demanding, both in terms of CPU cycles and RAM usage (GIF in particular is relatively RAM-heavy).

The MLA supports RLE as an option for bitmaps and resources, both when stored in internal and external memory.

When it comes to the more advanced GIF and JPG compression algorithms, the MLA provides support via an additional library module, called the "Image Decoders", that depends both on the Graphic library and the File System library to access images on mass storage media such as a micro SD card.

The Image Decoders module has its own configuration file (ImageDecoderConfig.h) where we can optimize the support required to achieve the smallest possible footprint and the most flexible application.

Coming Up

Choosing, formatting and laying out the right graphical resources for a user interface is often considered closer to an art form than an engineering task. This is even more true in embedded applications, as the usual memory and performance constraints apply while the number of tradeoffs multiply. Being aware of all these challenges and being knowledgeable of the tools and support that we can receive from the MLA is fundamental to delivering an effective product.

In a future column we will dig deeper into the low-level aspect of the serial Flash interface and files system support, looking at their use in graphics and other applications.

Stay tuned! ●

USER INTERFACE DESIGN FOR EMBEDDED APPLICATIONS

Lucio Di Jasio is EMEA Business Development Manager at Microchip Technology. He held various technical and marketing jobs within the company's 8, 16 and 32-bit divisions for the past 18 years. Lucio has published several books on programming for embedded control applications, and we have three copies of his book *'Graphics, Touch, Sound and USB, User Interface Design for Embedded Applications'* to give away at the end of the series. If you want to be in with a chance, please write to the Editor at svetlanaj@sjpbusinessmedia.com, mentioning the book in the heading.

```
...
/* Comment out the image formats which are not
required */
#define IMG_SUPPORT_BMP
#define IMG_SUPPORT_JPEG
#define IMG_SUPPORT_GIF

/* Comment out if output has to be given through a
call-back function */

/* If defined, the code is optimized to use only the
graphics driver, only 16-bit-565-color-format is
supported */
//#define IMG_USE_ONLY_565_GRAPHICS_
DRIVER_FOR_OUTPUT

/* If defined, the code is optimized to use only the
MDD file system */

//#define IMG_USE_ONLY_MDD_FILE_SYSTEM_
FOR_INPUT

/* If defined, the a loop call-back function is called
in every decoding loop so that application can do
maintenance activities such as getting data, updating
display, etc ... */
#define IMG_SUPPORT_IMAGE_DECODER_LOOP_
CALLBACK
...
```

Figure 4: Segment of ImageDecoderConfig.h

Software Defined Magnetic Sensor

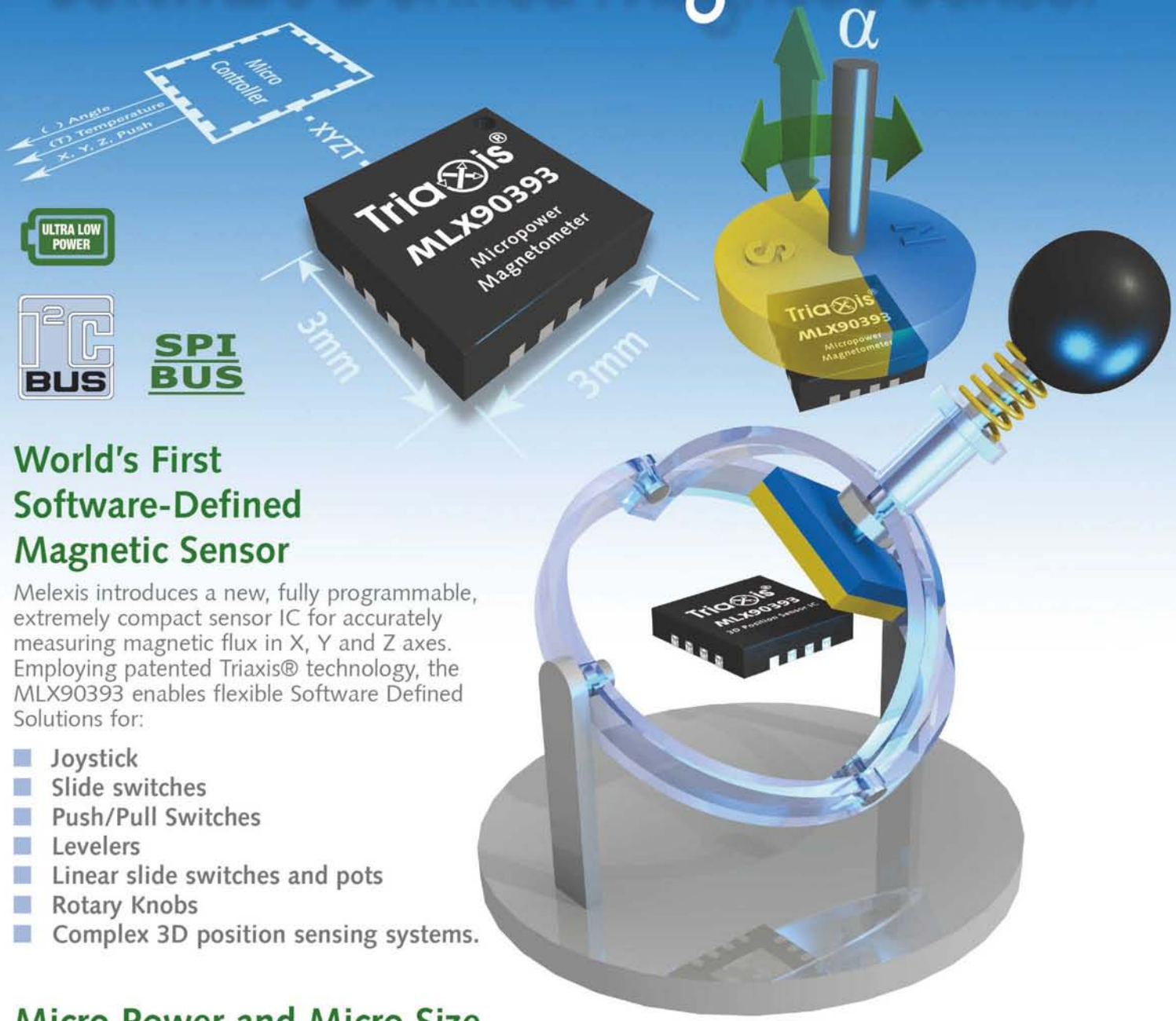

World's First Software-Defined Magnetic Sensor

Melexis introduces a new, fully programmable, extremely compact sensor IC for accurately measuring magnetic flux in X, Y and Z axes. Employing patented Triaxis® technology, the MLX90393 enables flexible Software Defined Solutions for:

- Joystick
- Slide switches
- Push/Pull Switches
- Levelers
- Linear slide switches and pots
- Rotary Knobs
- Complex 3D position sensing systems.

Micro Power and Micro Size

Suitable for micropower applications, the MLX90393 draws just 2.5µA of current when idle and features a "wake-up" on magnetic state change feature for intelligent magnetic sensor system behavior. Supporting an operational temperature range of -40°C to +85°C, the MLX90393 is supplied in a ultra small 3mm x 3mm QFN package.

Kickstart YOUR Software Defined Sensor NOW! EVB's and Example Code Available At:

www.melexis.com/MLX90393

We Engineer
The Sustainable Future.

Melexis
Microelectronic Integrated Systems

Determinism

MYK DORMER IS A SENIOR RF DESIGN ENGINEER AT RADIOMETRIX LTD **WWW.RADIOMETRIX.COM**

In an ideal world every radio link would have its own dedicated slice of spectrum allocated uniquely to it, but in our imperfect real world there are many occasions where more than one transmitter needs to share a single RF channel or frequency, for reasons that range from band regulation limits to the necessity to minimize hardware complexity due to mechanical or financial constraints.

A great deal has been written – and developed – about the mechanisms necessary to properly achieve that end, from sophisticated synchronized network architectures, where each message has its place in a carefully planned time-sharing arrangement, to "everybody shouts at once" systems, where random intervals between transmissions give a chance of at least some messages getting through, eventually.

I intend here to describe another, less well-known method: deterministic pattern signaling.

> Here, I intend to describe another, less well-known method: deterministic pattern signaling

Consider this fairly common low-power-radio application: a small number of "alarm" transmitters, which all need to send the state of their single "button" input to a central, single-output master receiver. Transmitters are battery-powered devices and need a long lifespan, while the central receiver can tolerate a (modest) constant current drain. As this is a simple system, the receiver has only one output, activated by a message from any of the transmitters – a very typical simple fire alarm or "machine stop" system; the radio equivalent of hard-wiring a number of buttons in parallel.

It would be possible to put a transceiver in every node, have the master send a periodic synchronizing message and time-divide the subsequent reply period between the transmitters. This approach is perfectly valid and is frequently used in more complicated networks, but it is also over-complex and draws power from the button batteries to remain synchronized.

A one-way unsynchronized system, with just a transmitter located at each button, is far less complex but suffers from a significant limitation: there is no activation at the receiver if two or more transmitters are active at the same time. The usual workaround for this situation is to set up a signaling rule by which every activated transmitter leaves a (pseudo) random delay between consecutive message transmissions. The upshot is that if any two transmissions collide, there is a (statistical) chance that the next time either transmitter sends a message they will not. Increasing the time between transmissions (or, in other words, the probability of a message being sent at any specific time) increases the likelihood of success.

Unfortunately, no matter what the random rule used, it is not possible to say that a transmission will definitely pass without collisions. With the right rule, the chance of failure can be made vanishingly small, but it never actually becomes zero.

For something like a light switch or an electric gate opener this is not an issue. In the event of a failed transmission, the user will simply repeat the activation, as often as necessary, to achieve success, but in a safety-critical application (the previously mentioned "machine stop" application) this is not an option.

There is an alternative. Instead of a (necessarily long) random interval between message re-transmissions, it is possible to use shorter cyclic patterns. By assigning a different pattern to each transmitter on the system (and carefully choosing the patterns), the designer can guarantee a successful collision-free activation within a known (and predictable) time-frame, even in the worst-case situation when every transmitter on system is activated. A series of examples will hopefully illustrate the point:

Let us imagine a two-transmitter system with a single output receiver.
Assume a further 50ms long transmit burst.
Signaling rule: Transmitter A leaves a 100ms gap between messages.
Transmitter B leaves a 150ms gap between messages.

If either transmitter is active in isolation, there are no collisions.

If both transmitters activate simultaneously, their first messages collide, but the second pair of messages will not.

In a worst-case situation, when transmitter A activates 25ms after transmitter B, the first and second messages overlap and are lost, but the third burst (and the fourth from transmitter A) is clear (as are the seventh and eighth from unit A, and the sixth from B, and so on, as the pattern repeats).

We can then add a third transmitter to this system. Transmitter C transmits continuously.

When transmitter C is operating, all messages from A or B will be blocked, but there is no pattern of A and/or B activations that will block every C message (and as this is a single output receiver system, it does not matter which transmitter message is received to initiate a valid "stop" action).

It can also be seen that there is a known worst-case activation time (in the example it is eight message periods or 0.4 seconds, which happens with only units A and B active).

Visualizing these patterns of messages and gaps is not that easy, especially as more transmitters are added to a system. While software modeling is entirely appropriate for this sort of task, I find that a literal physical scale model of the timing patterns, and the overlaps and collisions between them, can be easily made by working with strips of graph paper (with elapsed time represented as the X-axis across the length of the strip, and messages represented by shaded portions). This makes it very easy to see the inter-relationships between transmit patterns, and by sliding the strips relative to each other, the worst-case timings (and from that the worst-case activation times) can be readily seen.

This is a simple technique. It is not suited to all types of low-power networks (for example, it may not readily support multiple message/multiple output systems) and if the transmitter patterns are not judiciously chosen it will not work at all (some patterns of three or more transmitters will, in their worst cases, never yield a clear message). Indeed, with enough transmitters it is entirely possible that a viable set of signaling patterns will actually not exist at all.

On the other hand, it does provide an easy to understand solution to a commonly encountered low-power radio application, which can be implemented with very simple hardware. ●

POWERING SMART WEARABLE DEVICES

By Steve Knoth, Senior Product Marketing Engineer – Power Products
Linear Technology Corporation

From Google Glass to advanced fitness activity trackers, to heads-up imaging displays to blood pressure monitors, wearable devices have entered the military, industrial and high-end consumer markets. These devices are rapidly improving and becoming even "smarter". A "wearable" can be defined as a product that is worn by the user for an extended period of time and in some way, enhances the user's experience as a result of the product being worn. A "smart" wearable adds connectivity and independent processing capability to the device. It is estimated that the wearables market will grow to 130 million units by 2018 [Source: PwC, October 2014]. Wearables are divided into five application sub-categories: fitness/wellness (activity monitors, fitness bands, foot pods and heart rate monitors), healthcare/medical (pulse oximeters, hearing aids and blood pressure monitors), infotainment (smart glasses/goggles, smart watches and imaging devices), military (heads-up displays, exo-skeletons and smart clothing), and industrial (body-worn terminals) [Source: IHS Electronics and Media, 2013]. These categories have different market forces driving their adoption rates. In the wellness and medical segments, these include: rising life expectancy, the desire to prolong a healthy life and to reduce hospital stays. For military, it's the desire to improve situational awareness, maps/routes, combat efficiency and save lives. For industrial, the main drivers are improving production line efficiency and tracking capability. And finally, for infotainment, the exploding gaming market with cutting edge imaging and virtual reality, as well as the increasing number of devices able to connect wirelessly to smart phones to become part of the "internet of things" (IoT).

Smart Wearables Architecture and Problems

So, what's "under the hood" of your smart wearable device? Think of it as a miniature embedded system. The exact partitioning will obviously depend on the device itself, however, generally speaking the core architecture for a smart wearable is a combination of the following: a microprocessor or microcontroller or similar IC, some sort of micro-electromechanical sensors (MEMS), small mechanical actuators, Global Positioning System (GPS) IC, Bluetooth/cellular connectivity, imaging electronics, LEDs, computing resources, battery or battery pack, and support electronics.

A wearable unit's primary goals are to have a compact form factor, low weight for wearability/comfort and provide ultralow energy consumption in order to extend battery run time. Wearables are obviously "cool" products - however powering them efficiently and accurately while charging batteries with minimal current draw - is another matter entirely. Some of the key issues associated with powering smart wearables with ICs include the following:

- Low current consumption from the IC in a battery-powered device is paramount for increased run time. A micropower – or even better a nanopower – conversion IC is ideal.
- Some wearable device architectures use a multiple-battery approach, for example, 2xLithium 8.4V battery rather than a single-cell Lithium (4.2V). This increases capacity and gives longer system run time. However, a higher voltage IC is then required.
- A MEMS sensor requires power from a quiet regulated power source. Busy actuators may also benefit. An LDO works great for such rails since they have low output ripple.
- Bluetooth/RF connectivity system rails also require low noise. A low dropout regulator or, since output currents can be high, an LDO post-regulated switching regulator is a good choice.
- Processor power (the "brains" of the wearable). From TI OMAP, ARM Cortex MCUs, DSPs, GPS chips or FPGAs for example, have a variety of low-voltage rails, spanning low level to high currents. These can be powered by LDOs or switching regulators.
- Batteries need care and feeding so as to avoid overcharging which thus reduces battery cycle life. Accurate battery chargers with onboard termination algorithms ensure longer life for the cell(s).
- Compact size and low weight make the wearable device more comfortable for the user. ICs in compact packages provide small solution footprints, thus enabling the device to be offered in a small form factor.
- A feature-rich wearable product means many system rails. Multiple output regulators or power management integrated circuits (PMICs) may well fit the bill. Finally, compact ICs with battery chargers integrated onboard provide a higher level of integration and flexibility.

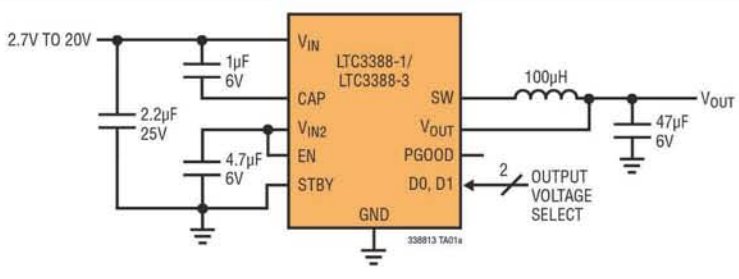

Figure 1: LTC3388-1/-3 Typical Application Circuit

Ultra-Low Iq IC Solutions

It is clear that an IC solution that solves the application needs, as well as the associated issues already discussed should have many of the following attributes:

- Ultra-low quiescent current, both in operating mode and shutdown
- Wide input voltage range to accommodate a variety of power sources

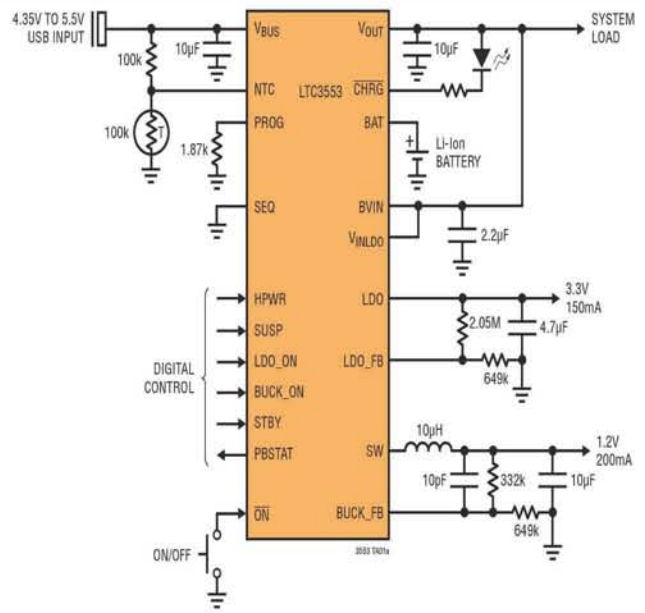

Figure 2: LTC3553 Simplified Application Schematic

- The ability to efficiently power multiple system rails
- Accurate battery charge voltage to prevent overcharging
- The ability to charge popular battery chemistries such as Lithium
- Simple and autonomous charging operation with onboard charge termination algorithms (no µC needed)
- Small and low profile solution footprints
- Advanced packaging for improved thermal performance and space efficiency

Fortunately, Linear's recent ultra-low Iq LTC3388/-x buck regulator family, and its LTC3553 combination buck regulator / LDO & single-cell Lithium battery charger PMIC have most of these attributes already.

The LTC3388 is an ultralow quiescent current synchronous buck converter than can deliver up to 50mA of continuous output current from a 2.7V to 20V input supply. The LTC3388's no-load operating current of only 720nA makes it ideal for a wide range of battery-powered and low quiescent power applications including "keep-alive" supplies and wearables. The LTC3388 utilizes hysteretic synchronous rectification to optimize efficiency over a wide range of load currents. It can offer over 90% efficiency for loads ranging from 15µA to 50mA and only requires 720nA of no load quiescent current in regulation, thereby extending battery life. The combination of a 3mm x 3mm DFN package (or MSOP-10) and only five external components offers a very simple and compact solution footprint for a wide array of low power applications. Figure 1 shows a typical LTC3388 application circuit.

For a Higher Scale of Integration – Use a PMIC

The LTC3553 is a micropower multi-function PMIC for portable Li-Ion/Polymer battery applications. The LTC3553 integrates a USB-compatible linear PowerPath manager, a standalone battery charger, a 200mA high efficiency synchronous buck regulator, a 150mA LDO and pushbutton control, all in a compact 3mm x 3mm QFN package, refer to Figure 2 for its typical application circuit. For applications operating with low currents in standby mode, the IC's pin-selectable Standby Mode reduces battery drain current to only ~12µA while maintaining regulation of all outputs, see Figure 3's graph for details. The LTC3553 is highly suited for personal navigation devices (PNDs), media players, portable medical and industrial devices and other small-battery portable device applications with small capacity batteries that consume low amounts of power. For similar applications that require a little higher power level and conversion efficiency, the LTC3554 is very similar except it offers 2x200mA buck regulators instead.

Conclusion

The smart wearables market is exploding and includes a wide variety of products for the health & fitness, medical, infotainment, military and industrial application spaces. The core architecture for a smart wearable device depends on the product type, but essentially boils down to a micro-controller, MEMS sensor(s), wireless connectivity, battery and support electronics. Powering a low-current wearable device can prove very challenging; however, Linear Technology offers a large portfolio of leading-edge products capable of very high performance at such low power levels. Devices like the ultra-low Iq LTC3388 energy harvesting buck regulator, and for a higher level of integration, the LTC3553 (or LTC3554) Lithium battery charger and buck regulator/LDO (Lithium charger + 2x200mA buck regulator) combination PMIC can enhance the operating life and overall performance of many future wearable devices.

Linear Technology (UK) Ltd
Tel: 01628 477066
Email: uksales@linear.com • www.linear.com

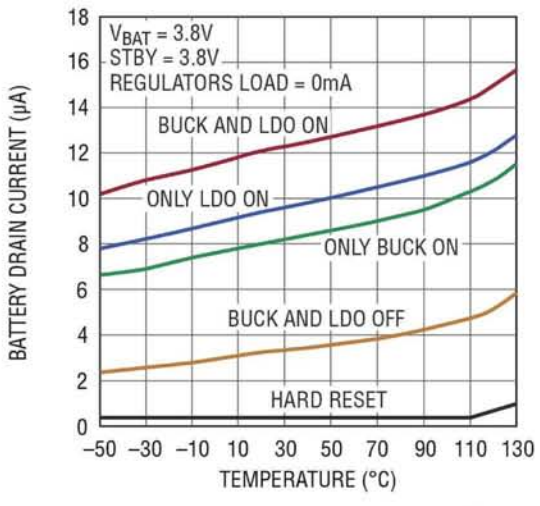

Figure 3: LTC3553 Battery Drain Current Operation

FOLDBACK CURRENT-LIMIT PROTECTION CIRCUIT FOR LARGE LOAD CURRENT LOW DROPOUT REGULATORS

LING-FENG SHI AND **FEI MA** FROM XIDIAN UNIVERSITY IN CHINA PRESENT A CURRENT-LIMIT PROTECTION CIRCUIT USED IN AN LDO WITH N-CHANNEL MOSFET ADJUSTMENT TRANSISTOR, FOR LOW POWER

A C/DC converters are widely used in many electronic systems, from industrial electronics to consumer devices and more. Low Dropout Regulators (LDOs) are linear regulators particularly useful in portable electronic systems due to their simple structure, low cost, low noise, low power consumption and high power supply rejection.

Quiescent current is the key factor in reducing power consumption in LDOs and optimizing their performance. At present, highly-integrated portable systems use large power-management chips for simplicity, but they consume a lot of power, especially when the output is overloaded or the circuit shorted. Such large output currents can permanently damage a transistor, so modern-day power management chips are used as current-limit protection circuits – an important aspect of their design.

The current limiting circuit function keeps the load current within a fixed range to protect the system or load when an output may be short-circuited or overloaded. DC/DC converters require such current limiting circuits. However, traditional current limiting circuits have issues with overcurrent shutdown and power consumption, so engineering developments have focused on addressing those.

Foldback current-limiting circuits combine a constant current-limiting circuit with a foldback circuit, offering high performance. With this type circuit, quiescent current is nearly the same for all load conditions, and power dissipation can be lowered to 61%.

This article presents a novel foldback current-limit protection circuit applied to LDOs, using an n-channel MOSFET as the power transistor. Maximum output current is set to 3.6A and maximum short-circuit current to 1.8A. At the same time, the circuit outputs a detection signal to check if V_{OUT} is within the 90% of its normal range. If it is, a detection signal P_{GOOD} is sent out after a delay of 1.5ms.

Traditional Current-Limiting Circuits

There are two common methods for sampling output currents in CMOS LDOs. As shown in Figure 1, one of them is to directly connect a small value resistor to the power transistor.

The other method is shown in Figure 2, where a small-value transistor is connected to the power transistor via the gate and source terminals respectively. The output current and the transistor current have a proportional relationship so the current can be sampled.

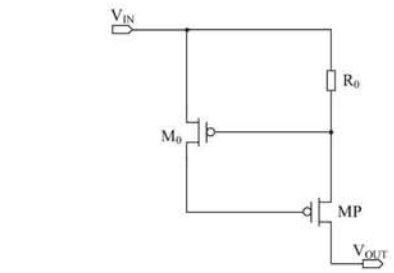

Figure 1: Traditional current-limit circuit

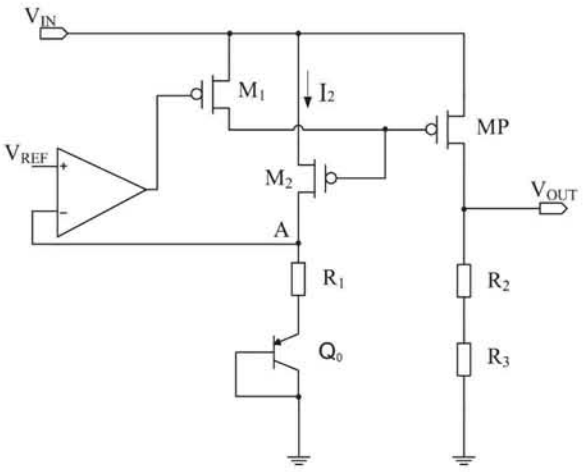

Figure 2: Improved current-limit circuit

In Figure 1, MP is an adjustment transistor and R_0 is a sampling resistor. The protection circuit consists of R_0 and M_0. Since the current flowing through R_0 is approximately equal to the output current I_{OUT}, the voltage drop at R_0 is proportional to the output current I_{OUT}. M_0's gate-source voltage V_{GS1} is:

$$V_{GS1} = -V_{R_0} = -R_0 I_{OUT} \quad (1)$$

The gate voltage of the regulator MP is controlled by the system's amplification circuit under normal conditions and when M_0 is off. When the output current I_{OUT} increases to a certain value, $V_{GS1} < V_{TP}$, M_0 turns on, the gate of MP is pulled high; limiting the output current to a certain value, achieving overcurrent protection.

Due to the voltage drop across sampling resistor R_0, this protection circuit decreases the system's conversion efficiency, especially in the case of heavy loads. With heavy loads, system loss is not only more serious, but also leads to higher dropout voltages. In addition, the sampling resistor value needs to be highly accurate, even though the integrated resistor is very sensitive to process and temperature changes, which tends to affect the accuracy of the current limit protection.

As shown in Figure 2, MP is the adjustment transistor and the current-limit circuit consists of a comparator circuit, p-channel MOSFETs (M_1 and M_2), a sampling resistor R_1 and a transistor Q_0. The comparator's positive terminal is the reference voltage V_{REF}. M_2 samples the output current I_{OUT} flowing through the adjustment transistor MP so the leakage current I_2 of M_2 reflects the output current. The voltage at node A is:

$$V_A = R_1 I_2 + V_{EB} \quad (2)$$

where V_{EB} is the voltage between the emitter and base of Q_0.

Under normal operating conditions, the voltage at node A is $V_A < V_{REF}$, the comparator output is high and the M_1 transistor is off. Gate voltage of the adjustment transistor MP is determined by the LDO-system's amplification circuit. When the output current reaches a certain value, the voltage at node A is $V_A > V_{REF}$; then, the comparator's output goes low and M_1 is on, so the regulator MP's gate is pulled high. Finally, the output current is clamped at a certain value to achieve overcurrent protection.

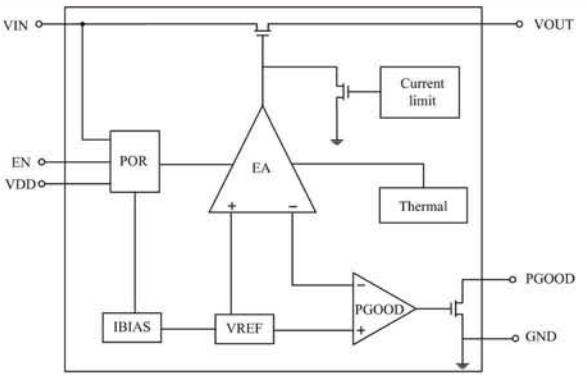

Figure 3: Structure of the proposed LDO

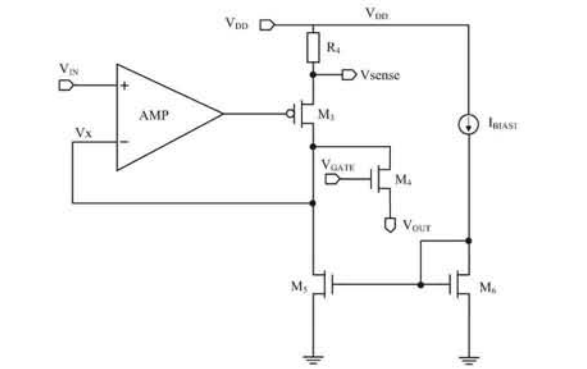

Figure 4: The proposed sampling circuit

Compared to Figure 1, sampling resistor R_1 of the current-limit circuit in Figure 2 and regulator MP are not connected in series so there's no voltage drop, which increases conversion efficiency. However, current flowing through the transistor is limited to a relatively large value when the system has overcurrent, which leads to large power consumption. This problem can be solved with our suggested foldback current-limit circuit.

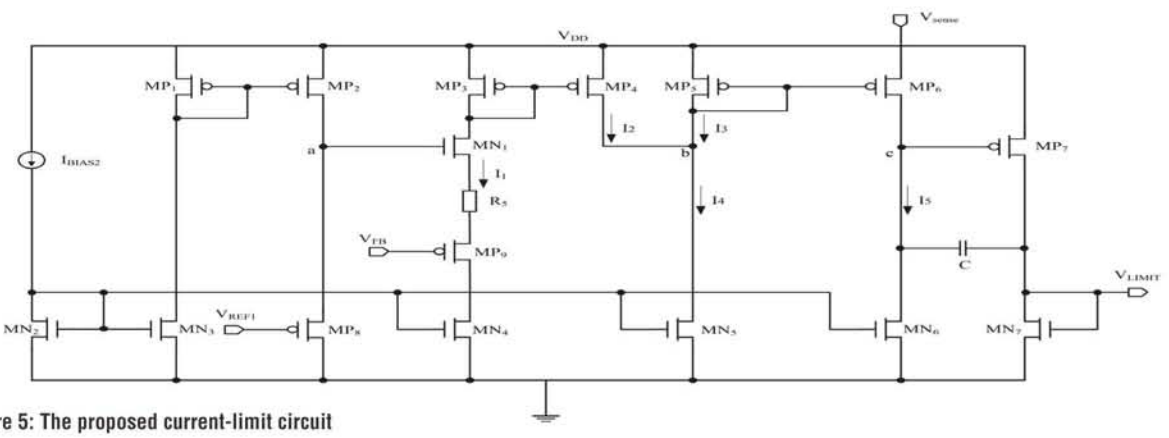

Figure 5: The proposed current-limit circuit

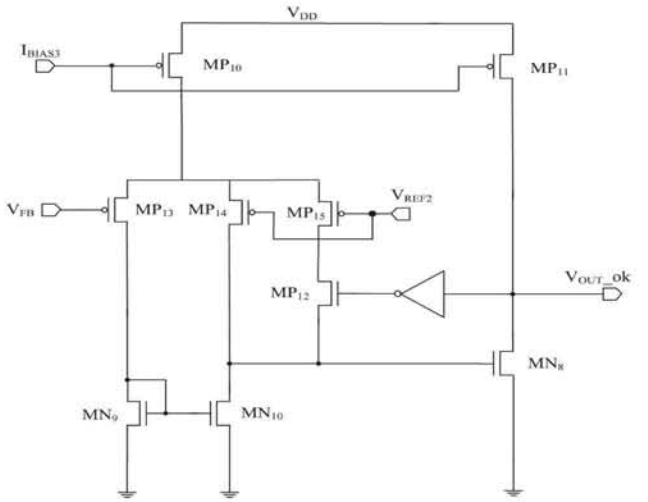

Figure 6: Output voltage detection circuit

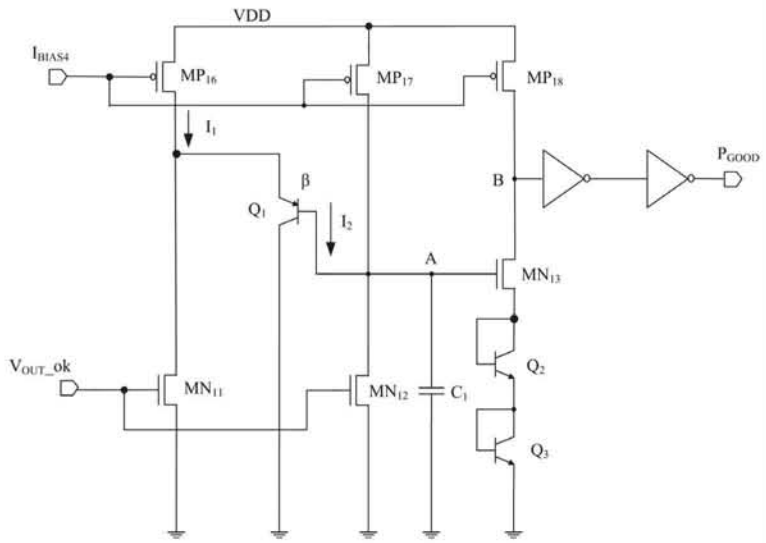

Figure 7: Detection signal delay circuit

Circuit Description

The proposed LDO consists of a voltage reference, current reference, error amplifier, pass transistor, power-on reset, thermal protect circuit, feedback current limit and power-good circuit, as shown in Figure 3. The system involves VIN, EN, VDD, VOUT, ADJ, PGOOD and GND − seven pins. The LDO uses the n-channel MOSFET as a pass transistor.

The foldback current-limit circuit consists of a sampling circuit and a current-limit circuit, shown in Figures 4 and 5, respectively. Figure 4 is the block diagram of the proposed sampling circuit, which consists of a sampling n-channel MOSFET M_4, a p-channel MOSFET M_3 error amplifier, a sampling resistance R_4, and a current mirror consisting of M_5 and M_6 with a ratio of 1:1.

To ensure the sampling transistor and power transistor have the same voltage on each port, the gate terminal of M_4 and the power transistor are connected to the same driving voltage V_{GATE}, and the source terminal of M_4 connects to the output V_{OUT}; the AMP makes V_{IN} followed by the V_x voltage.

In our project, LDO load capability is 3A and the current limit is set at 3.6A, so resistance R_4 is low. The ratio of M_4 in Figure 4 to MN_1 in Figure 3 is set to be 1: K, where K is usually several thousand (1,000 for the purposes of this article). As such, the sampled current I_S value can be expressed as:

$$I_S = \frac{1}{K} I_{load} \tag{3}$$

The sampling current through R_4 is converted to voltage and can be obtained with:

$$V_{sense} = V_{DD} - R_4(I_S + I_{BIAS}) \tag{4}$$

where I_{BIAS} is the current flowing through M_5 and is the same as the bias current I_{BIAS1}.

Figure 5 shows the block diagram of the proposed current-limit circuit. V_{REF1} is a reference voltage of 0.8V, and MP_8 provides DC operating voltage for MN_{10}. When I_{OUT} < 3.6A, V_{FB} is about 0.8V and MP_9 conducts weakly, so I_1 is small. Transistors MP_3 and MP_4 are mirrored current, and transistors MN_7 and MN_8 are current mirror, thus I_1 and I_2 are equal and the drain current of MN_7 and MN_8 is I_{BIAS2}. If the output current does not exceed the current limit 3.6A and the pull-up effect of MP_6 is stronger than MN_8's pull-down, the point c remains at a high level and MP_7 is off so that no current flows through MN_9. As such, the current-limit circuit does not work.

As the load current increases, the pull-down effect of I_5 gradually increases so the pull-up effect of MP_6 also increases gradually. With this, V_c gradually reduces, turning MP_7 on, and V_{LIMIT} gradually increases, achieving limiting.

Almost all the current flowing through R_4 flows into M_3 (see Figure 4); so the current through MP_6 can be ignored (see Figure 5). When the current limit value is reached, I_4 and I_5 are equal in Equation 5, which can be written as:

$$I_5 = I_4 = I_2 + I_3 \tag{5}$$

where:

$$I_5 = \beta(\frac{W}{l})_{MP6}(V_{sense} - V_b - V_{th})^2 \tag{6}$$

and where β is the transconductance of the transistor, $(\frac{W}{l})_{MP6}$ is the width-to-length ratio of MP_6, and V_{th} is the threshold voltage of the transistor. So, V_{sense} can also be expressed as:

$$V_{sense} = \sqrt{\frac{I_5}{\beta(\frac{W}{l})_{MP6}}} + V_b + V_{th} \tag{7}$$

and for MP_5 as:

$$I_3 = \beta(\frac{W}{l})_{MP5}(V_{DD} - V_b - V_{th})^2 \quad (8)$$

Combining Equations 3-8 yields:

$$I_{limit} = \frac{K}{R_4}\left(\sqrt{\frac{I_3}{\beta(\frac{W}{l})_{MP5}}} - \sqrt{\frac{I_5}{\beta(\frac{W}{l})_{MP6}}}\right) - I_{BIAS} \quad (9)$$

The load resistance and output voltage decrease, resulting in a gradually reduced feedback value V_{FB}. The conductive capability of MP_9 gradually increases when the load current reaches the current limit; I_1 increases as the load resistance decreases and I_2 increases because of the mirror effect.

From Equation 8 it can be seen that I_3 is gradually reduced and V_b gradually increased. As the ratio of MP_5 and MP_6 is chosen as 1:M, the value of M can be adjusted to make the increase of V_b greater than that of V_{sense}. Therefore, based on Equation 9 it can be determined that the current limit decreases as I_3 decreases, and the goal of foldback current limiting can be achieved.

When the output voltage is $V_{OUT} < 0.2V$, MP_9 fully conducts and the value of I_1 is at a maximum. As I_3 remains essentially unchanged, it keeps the output current at 1.8A.

Self-Inspection Function

By comparing the feedback signal V_{FB} of the output voltage V_{OUT} with the reference voltage V_{REF2}, it can be determined whether the output is normal and reaches 90% of the predetermined value, or not. The output of the detection circuit is sent out, and as it enters the transistor base terminal it charges the capacitor with a delay of 1.5ms.

The output voltage detection circuit and the detection signal delay circuit are shown in Figures 6 and 7, respectively.

Current flowing through MP_{13} is greater than that through MP_{14} when V_{FB} is not established and the V_{FB} level is lower than V_{REF2}, which is shown in Figure 6. The relationship of the currents is shown in the following equation:

$$I_{MP13} = I_{MN11} = I_{MN12} > I_{MP14} \quad (10)$$

The gate of MN_{13} is pulled low so MN_{13} cuts off. Meanwhile, the output voltage detection signal, V_{OUT_OK}, is high. When V_{FB} gradually increases to more than V_{REF2}, it makes MP_{14}'s drain level and MN_{13}'s gate level pull up. Then, MN_{13} conducts (see Figure 6) and the output voltage detection signal, V_{OUT_OK}, goes low. To prevent turning point oscillation, hysteresis is generated by the MOSFET MP_{12} and MP_{15}.

Figure 7 shows the block diagram of the detection signal delay circuit. The output voltage detection signal V_{OUT_OK} is high and MN_{14} and MN_{15} are conductive, which makes point A and the gate of MN_{16} low, so MN_{16} does not conduct, and point B goes high. The output detection signal P_{GOOD} outputs a high.

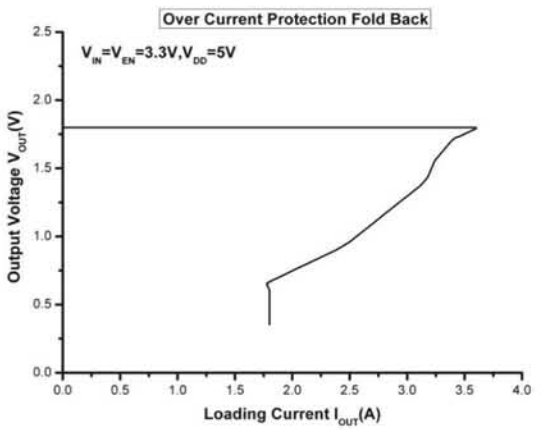

Figure 8: Simulation curve of the foldback current-limit circuit

With V_{FB} gradually established, output voltage detection signal V_{OUT_OK} is at a low level, and both MN_{14} and MN_{15} cut off so that current I_1 of MP_{19} flows through transistor Q_1. Base current $I_2 = I_1/\beta$ constitutes the capacitor C_1's charging current. The voltage at point A for a given time can be expressed as:

$$\frac{I_1 \times t}{\beta} = CV_A \quad (11)$$

When point A's level is $V_A > V_{th13} + 2V_{be} + V_{on(MN13)}$, MN_{13}, Q_1 and Q_2 turn on, pulling point B low, while detection signal P_{GOOD} flips from high to low.

Dividing detection signal P_{GOOD} with output voltage detection signal V_{OUT_OK} gives delay time t:

$$t = \frac{(V_{th13} + 2V_{be} + V_{ON(MN13)})C\beta}{I_1} \quad (12)$$

where V_{th13} is the threshold voltage of MN_{13}, V_{be} is the transistor base-emitter voltage, $V_{ON(MN13)}$ is the voltage drop of MN_{13}, β is the current amplification ratio of the transistor and I_1 includes the current on MP_{17} and I_2.

Test Results

The foldback current-limit circuit in this article was simulated and verified based on a 0.35μm 5V CMOS process, for a chip area of 1.6 × 0.9mm^2. The circuit was verified by Hspice simulation and with a tapeout test. The simulation result is shown in Figure 8. It can be seen that the value of the current limit decreases as the load resistance decreases from the initial 3.6A, reduced to 1.8A at short-circuit.

Figure 9 shows simulation results of the output voltage detection signal V_{OUT_OK}. When V_{FB} reaches V_{REF2}, a transition occurs and the detection signal goes from high to low.

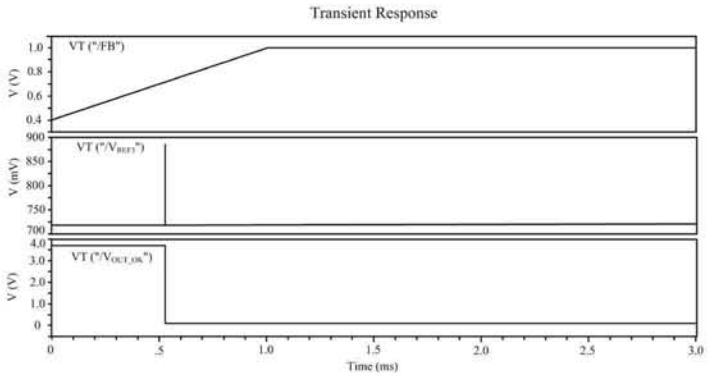

Figure 9: Simulation curve of the output detection signal

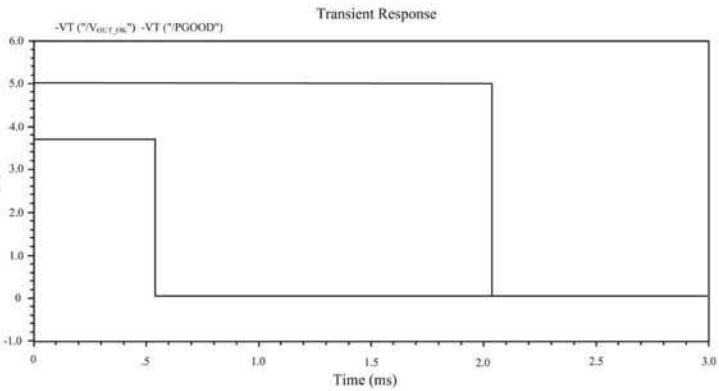

Figure 10: Simulation curve of the detection signal delay

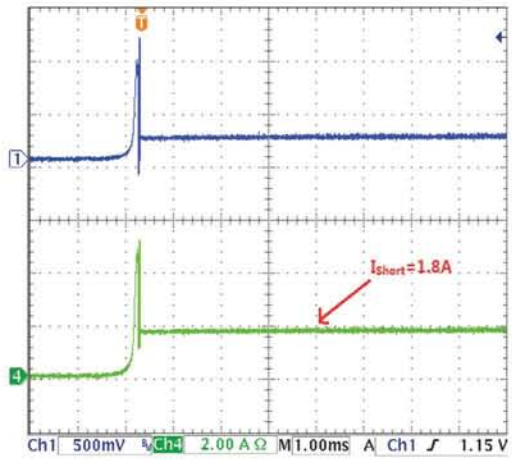

Figure 11: Test results of the short-circuit current

Figure 10 shows simulation results of the time delay circuit. It can be seen that when detection signal V_{OUT_OK} is output, a transition occurs, and the same goes for detection signal P_{GOOD} (but after 1.5ms), which goes from high to low.

Figure 11 illustrates the current when short circuited. When the output is shorted, the system's short-circuit current is 1.8A.

OLSON®

UK's No.1 IEC Connection

CALL OUR SALES HOTLINE

020 8905 7273

VISA MasterCard Maestro

24 HOUR DELIVERY SERVICE

ISO 9001 REGISTERED FIRM

GB 1907

OLSON ELECTRONICS LIMITED
OLSON HOUSE, 490 HONEYPOT LANE, STANMORE, MIDDX HA7 1JX
TEL: 020 8905 7273 FAX: 020 8952 1232
e-mail: sales@olson.co.uk web site: http://www.olson.co.uk

MICROCONTROLLER-CONTROLLED ELECTRONIC CIRCUIT

FOR FAST MODELLING OF CHAOTIC EQUATIONS

SELCUK COSKUN, **SINAN TUNCEL**, **IHSAN PEHLIVAN** AND **AKIF AKGUL** FROM SAKARYA UNIVERSITY IN TURKEY CREATE AN ELECTRONIC CIRCUIT THAT WILL HELP CHAOTIC SYSTEM DEVELOPMENT AND CALCULATIONS

Researchers working on disciplines such as electronics, computing, electrics, physics and mathematics tend to rely on chaotic systems to demonstrate different sophisticated dynamic behaviours. Chaotic circuits have a sophisticated structure and their realization is complex, but there aren't many other techniques that allow the modelling of such systems.

We have developed a microcontroller-controlled circuit to enable users to set up chaotic circuits fast and easily, especially for circuits with initial conditions. The inclusion of initial conditions in the electronic development of chaotic systems may be necessary because of the system's structure.

Circuit Features

This microcontroller-controlled circuit is of modular design, allowing chaotic circuits to be set up fast and flexibly. The initial condition values can be adjusted accurately with potentiometers, and monitored via the computer interface.

Only one source is used for the initial condition and supply voltages, which simplifies the experimental equipment, speeding up the process.

There is no need to use a multimeter to measure voltage and resistance, and non-standard resistance values (e.g. 14.46 kohms) can be accurately adjusted by multi-turn trimpots.

The system consists of three main blocks:

1. Chaotic circuit block;
2. Voltage regulator block;
3. Microcontroller and interface program block.

The chaotic circuit block is where continuous time chaotic equations, consisting of elements like multipliers, inverters and integrators, are formed. Here, the circuit includes five multipliers, five inverters and five integrator modules. Having these blocks simplifies setting up a chaotic circuit.

The voltage regulator block uses only one symmetrical power source. Analog circuit elements, supply voltages and initial condition voltages used in the circuit are adjusted with a voltage regulator in this part. The potentiometers shown in Figure 2 are used to adjust the initial condition voltages. The switching circuit that cancels the initial-condition voltages necessary to run the chaotic circuit and which supplies voltage to the analog circuit elements, is also in this section.

Supervision of the microcontroller and interface program block

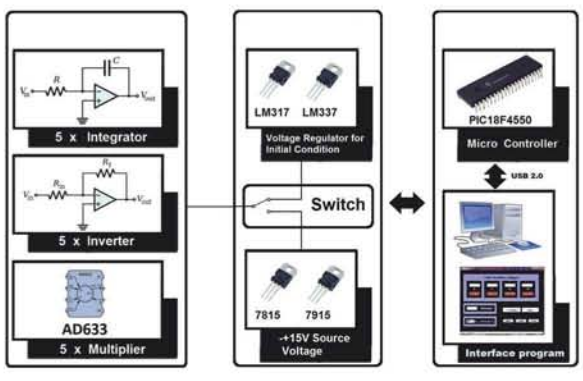

Figure 1: Block diagram of the computer-controlled electronic circuit

Figure 2: This circuit can be controlled by a computer or microcontroller

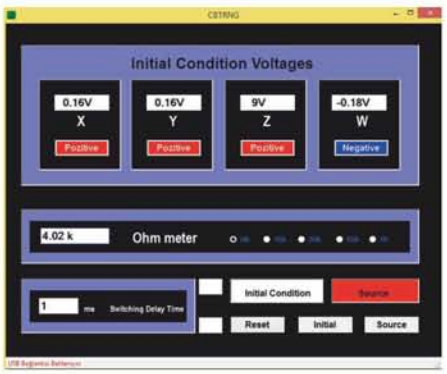

Figure 3: Screenshot of the computer interface program

is provided by a different program. The microcontroller reads the resistance values and initial condition voltages via ADC channels, and transfers them to the interface program via a USB port to drive and operate the chaotic circuit. The microcontroller we used is a PIC18F4550.

Thanks to the computer interface program, initial-condition voltages and resistance values can be accurately monitored. Whether the initial conditions will be positive or negative is determined by buttons on the interface program. Switching delay time goes into the "Switching Delay Time" box. After the values are entered, the "initial" button is pressed and initial conditions are applied to the chaotic circuit. Then the "source" button is pressed and a voltage is supplied to the system.

The interface program was created with Microsoft Visual Studio C Sharp. Figure 3 shows a screenshot of the interface program.

Sample Chaotic System Realization

Equations belonging to the chaotic Chen system chosen for the application are as follows:

$$\dot{x} = a \cdot (y - x)$$
$$\dot{y} = (c - a) \cdot x - x \cdot z + c \cdot y$$
$$\dot{z} = x \cdot y - b \cdot z$$

Typical parameter values are a = 35, b = 3, c = 28. Because the dynamic limits of the Chen system exceed the voltage limits of the power source in the circuit, the x, y and z variables need to be scaled. If the new variables are x/10, y/10 and z/10, the Chen equations whose circuit is to be set up will take the following form:

$$\dot{x} = a \cdot (v - u)$$
$$\dot{y} = (c - a) \cdot u - 10 \cdot u \cdot w + c \cdot v$$
$$\dot{z} = 10 \cdot u \cdot v - b \cdot w$$

The designed electronic circuit schematics of the scaled Chen system are shown in Figure 4.

The hardware setup for the sample application performed with the Chen system is shown on Figure 5. Detailed oscilloscope prints are shown in Figure 6. The initial conditions were taken to be x (0) = 0.16, y (0) = 0.16 and z (0) = 9V. ●

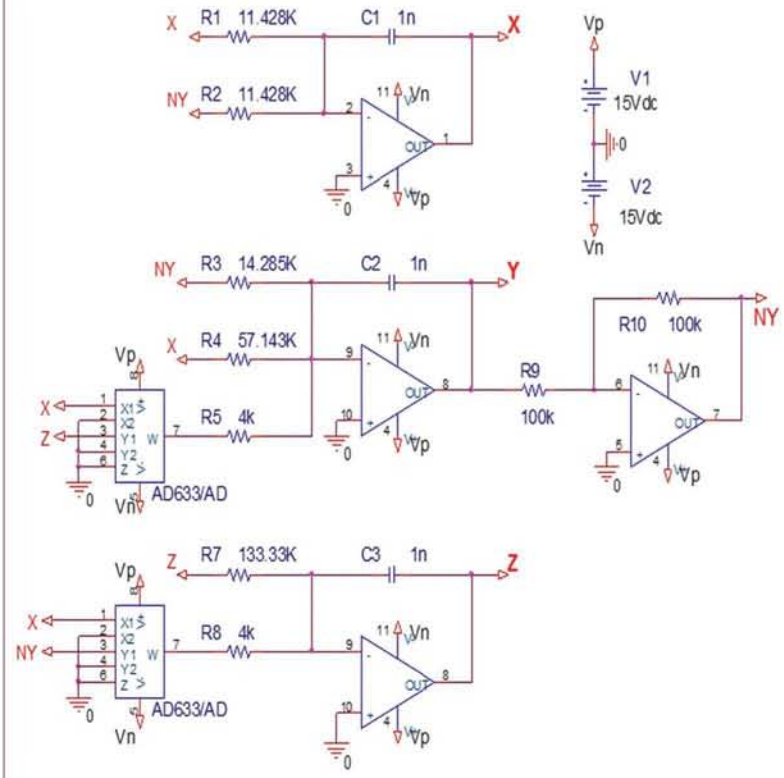

Figure 4: Circuit schematics of the scaled Chen system

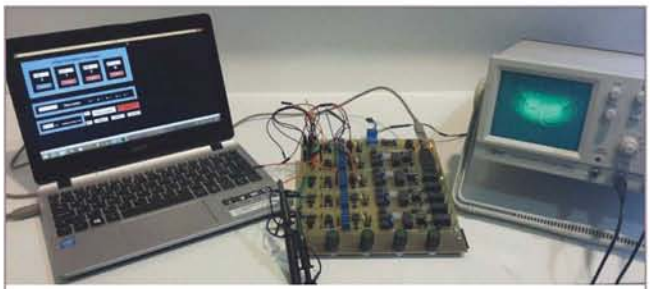

Figure 5: Realization of the chaotic Chen system with computer-controlled electronic circuit

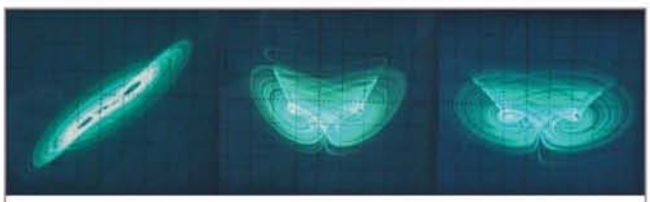

Figure 6: Oscilloscope outputs of the chaotic Chen system circuit

RADIOMETRIX

www.radiometrix.com

Frequency Programmable Narrow Band Transmitter

New range of highly flexible, frequency programmable, RF power adjustable radios.

True Narrow Band FM performance, available on user/factory programmable custom frequencies between 425MHz & 470MHz. Matching receiver available.

VISIT http://radiometrix.com/content/ntx2b

CALL +44 (0)20 8909 9595 *REAL RADIOS FOR REAL APPLICATIONS*

NEW! PS12MK /PS20MK Series IP67 rated power supplies

Features

- 90-264VAC universal AC input
- Compact dimensions PS12MK 56 x 39 x 26mm and PS20MK 64 x 47 x 28mm
- PS12MK 12 Watts & PS20MK 20 Watts
- Single DC outputs of 5, 9, 12, 15 or 24V
- IP67 fully encapsulated and waterproof
- Fixing holes for wall or chassis mounting
- Input and output connectors optional
- No Load Power Consumption ≤0.3W max
- EN60950 & EN55022 safety & EMC standards
- Ideal for CCTV or LED applications
- Class II safety, no earth connection required

POWER SOLVE

www.powersolve.co.uk
Email: sales@powersolve.co.uk Tel: 44-1635-521858

VOLTAGE-MODE MULTIFUNCTIONAL FILTER EMPLOYING TWO DO-CCII AND TWO GROUNDED CAPACITORS

FIRAT YUCEL FROM AKDENIZ UNIVERSITY AND **ERKAN YUCE** FROM PAMUKKALE UNIVERSITY, BOTH IN TURKEY, PRESENT THEIR DESIGN OF A VOLTAGE-MODE MULTIFUNCTIONAL FILTER USING TWO DUAL-OUTPUT SECOND-GENERATION CURRENT CONVEYORS

Analog filters are widely used in a number of applications, including communications and instrumentation, to eliminate unwanted signals. It is well-known that current-mode (CM) active devices such as second-generation current conveyors (CCIIs) offer wider bandwidth, higher linearity and greater dynamic range, and require fewer active devices when compared to their voltage-mode (VM) counterparts, such as operational amplifiers.

We have now created a VM multifunctional filter that can simultaneously realize lowpass (LP), bandpass (BP) and highpass (HP) responses from the same topology, and without the need for any critical passive-component matching conditions. However, it does require extra circuitry to provide notch and allpass filter responses, and it also doesn't have high input and low output impedances, so extra buffers are needed.

Circuit Description

A DO-CCII is defined by the following matrix equation:

$$\begin{bmatrix} V_X \\ I_Y \\ I_{Z+} \\ I_{Z-} \end{bmatrix} = \begin{bmatrix} \beta & 0 \\ 0 & 0 \\ 0 & \alpha \\ 0 & -\gamma \end{bmatrix} \begin{bmatrix} V_Y \\ I_X \end{bmatrix} \quad (1)$$

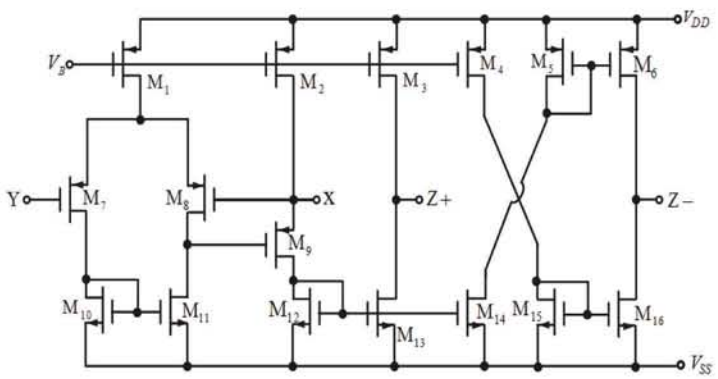

Figure 2: Internal structure of the DO-CCII

Transistor Type	W / L
PMOS transistors, M1-M8	41.6 µm/0.52 µm
PMOS transistor, M9	83.2 µm/0.52 µm
NMOS transistors, M10-M16	13.0 µm/0.52 µm

Table 1: Aspect ratios of the MOS transistors of the DO-CCII in Figure 2

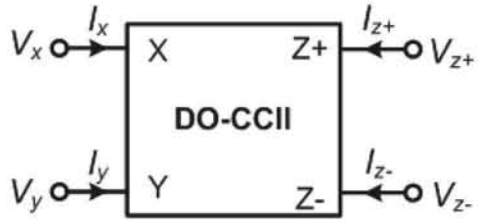

Figure 1: Electrical symbol of the DO-CCII

where β is a frequency-dependent non-ideal voltage gain, α and γ are frequency-dependent non-ideal current gains, and ideally should all be unity. At sufficiently low frequencies, α, β and γ can be presented as $\alpha = 1 - \varepsilon_\alpha$ ($|\varepsilon_\alpha| << 1$), $\beta = 1 - \varepsilon_\beta$ ($|\varepsilon_\beta| << 1$) and $\gamma = 1 - \varepsilon_\gamma$ ($|\varepsilon_\gamma| << 1$), where ε_α, ε_β and ε_γ are tracking errors of the associated gains and are ideally zero. The electrical symbol of the DO-CCII is shown in Figure 1.

The internal structure of the DO-CCII used in our simulations is shown in Figure 2, first suggested by W. Surakampontorn et al. It is assumed that all the MOS transistors in Figure 2 are operated in saturation region, and connected so as to prevent any body effects.

The Proposed Voltage-Mode Multifunctional Filter

The proposed VM filter is shown in Figure 3. Here, the ideal BP, LP and HP transfer functions (TFs) can be respectively found as follows:

$$\frac{V_{BP}}{V_{in}} = -\frac{C_2 R_3 s}{D(s)} \quad (2a)$$

$$\frac{V_{LP}}{V_{in}} = \frac{1}{D(s)} \quad (2b)$$

$$\frac{V_{HP}}{V_{in}} = \frac{C_1 C_2 R_1 R_3 s^2}{D(s)} \quad (2c)$$

where D(s) is described as the characteristic equation of the filter, given as:

$$D(s) = 1 + C_2 R_3 s + C_1 C_2 R_1 R_3 s^2 \quad (3)$$

Non-ideal BP, LP and HP TFs of the proposed filter are respectively evaluated as:

$$\frac{V_{BP}}{V_{in}} = -\frac{\alpha_2 C_2 R_1 s}{D_n(s)} \quad (4a)$$

$$\frac{V_{LP}}{V_{in}} = \frac{\alpha_1 \alpha_2}{D_n(s)} \quad (4b)$$

$$\frac{V_{HP}}{V_{in}} = \frac{(\gamma_2 - \alpha_2 \gamma_1) C_2 R_3 s + \gamma_2 C_1 C_2 R_1 R_3 s^2}{D_n(s)} \quad (4c)$$

where $D_n(s)$ is described as:

$$D_n(s) = \alpha_1 \alpha_2 \beta_2 + C_2 R_3 s + C_1 C_2 R_1 R_3 s^2 \quad (5)$$

Angular resonance frequency (ω_{on}) and quality factor (Q_n) derived from $D_n(s)$ in Equation 5 are respectively calculated as:

$$\omega_{on} = \sqrt{\frac{\alpha_1 \alpha_2 \beta_2}{C_1 C_2 R_1 R_3}} \quad (6a)$$

$$Q_n = \sqrt{\frac{\alpha_1 \alpha_2 \beta_2 C_1 R_1}{C_2 R_3}} \quad (6b)$$

Simulation Results

Simulations of the proposed filter are performed using the SPICE program with 0.13µm IBM CMOS technology parameters. Symmetrical DC power supply voltages are selected as ±0.75V. Bias voltage V_B in Figure 2 is chosen as 0.37V. Aspect ratios (W/L) of the MOS transistors of the DO-CCII in Figure 2 are given in Table 1. The passive components of the filter in Figure 3 are selected as $R_1 = R_2 = R_3 = 1k\Omega$ and $C_1 = C_2 = 50pF$, resulting in $f_o \cong 3.18MHz$ and $Q = 1$.

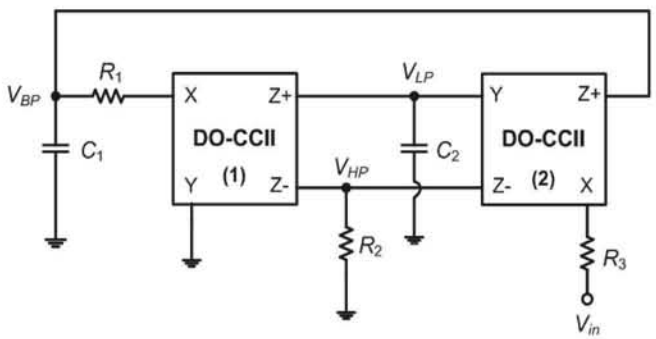

Figure 3: The proposed voltage-mode multifunctional filter

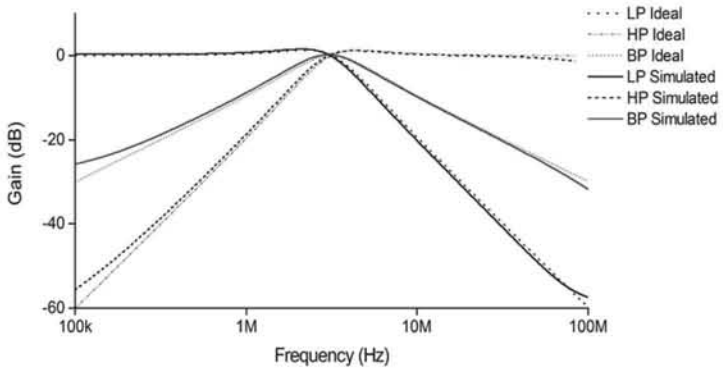

Figure 4: Gain responses of the proposed filter

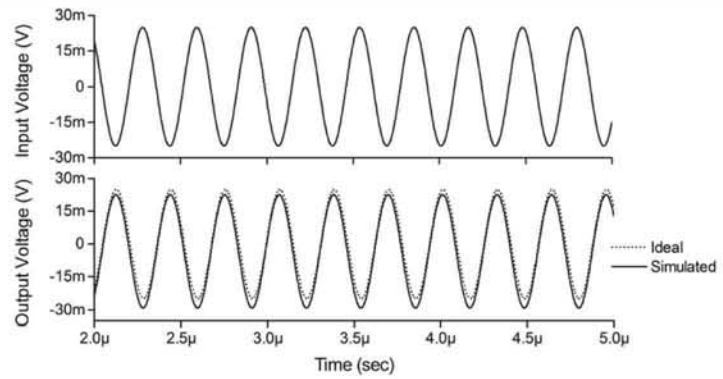

Figure 5: Time-domain bandpass response for the proposed filter

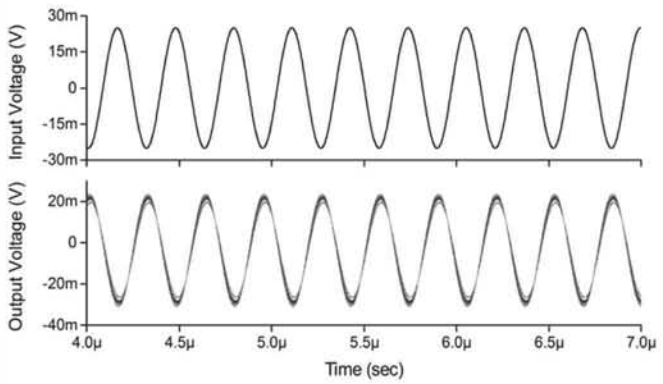

Figure 6: Monte Carlo analysis of the proposed filter with different resistor values R_1, R_2 and R_3

Gain responses of the proposed filter in Figure 3 are shown in Figure 4. Ideal and simulated results of the gains are close to each other.

A sinusoidal input signal with peak value of 25mV at the

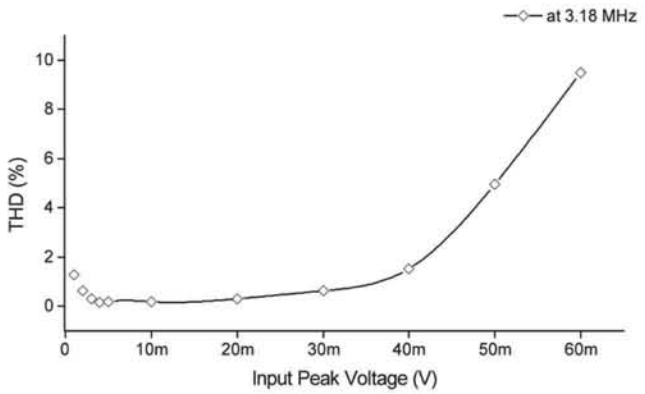

Figure 7: THD against sinusoidal input signal peak value for the proposed filter

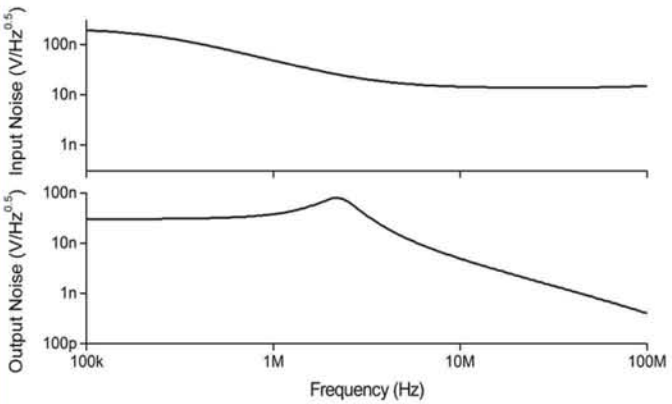

Figure 8: The proposed fitler's input and output noise versus frequency

resonance frequency is applied to the proposed filter in Figure 3. The input and corresponding ideal and simulated time-domain BP filter are shown in Figure 5.

A Monte Carlo analysis is performed with twenty runs for 10% variations of the resistors R_1, R_2 and R_3 for the proposed filter, where a sinusoidal input signal with peak value of 25mV at the resonance frequency. The input and corresponding BP output responses are shown in Figure 6.

Total power dissipation of the proposed filter is calculated in the simulations as 1.11mW. For the BP responses of the proposed filter, the total harmonic distortion (THD) variations with respect to peak value of the applied sinusoidal signal at the resonance frequency are shown in Figure 7; the respective input and output noise are shown in Figure 8.

Going Forward

The proposed filter does not have high input or low output impedances. Time domain and frequency domain simulation results confirm our theory; however, there is a small discrepancy between the ideal and simulation results, which arises from non-idealities of the DO-CCIIs, such as frequency-dependent non-ideal gains and parasitic impedances. ●

NEW, HIGH-PERFORMANCE, SECOND-GENERATION, CURRENT-CONTROLLED CURRENT CONVEYOR

ZHANG XIN, WANG CHUNHUA AND **JIN JIE** FROM THE COLLEGE OF INFORMATION SCIENCE AND ENGINEERING AT HUNAN UNIVERSITY IN CHANGSHA, CHINA, PRESENT A NOVEL HIGH-PERFORMANCE CMOS CURRENT-CONTROLLED CURRENT CONVEYOR (CCCII)

The current-mode component second-generation current conveyor (CCII) is a versatile and flexible building block in current-mode analog circuit design, including analog filters, oscillators, chaos generators and active inductance among others. However, its two main disadvantages are its large voltage transfer offset and lack of electronically-tunable characteristics.

Electronically-adjustable features can easily be achieved with CMOS-controlled second-generation current conveyor , or CCCII, where conventional BJT structures offer low noise and high operating frequency. CCCII implementation based on BiCMOS technology offers two main advantages: high integration density and low power consumption due to the CMOS technology, and high speed and strong current driving ability like BJT circuits. The disadvantage, however, is its incompatibility with CMOS VLSI technology.

CCCII based on an MOS translinear loop and CCCII based on MOS balanced differential pairs are compatible with CMOS VLSI technology, but the former has disadvantages of unsymmetrical dynamic range and strict restrictive conditions for its fabrication, whereas the latter has a poor input voltage range and low linearity.

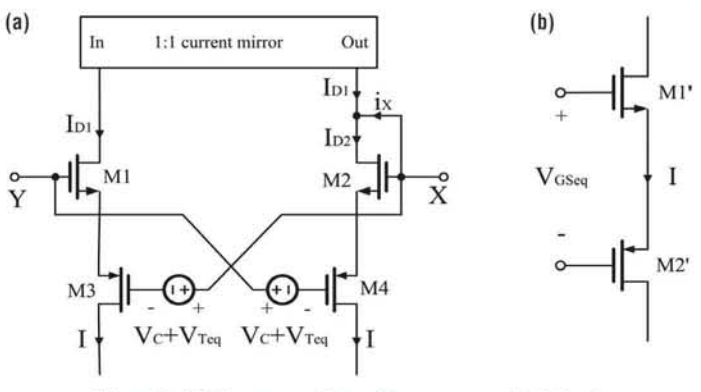

Figure 2: CMOS compound transistor cross-coupled circuit: (a) cross-coupled circuit; (b) CMOS compound transistor

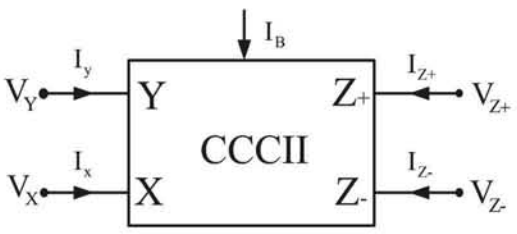

Figure 1: CCCII circuit symbol

Circuits using vertical n-p-n and p-n-p transistors to convey signals are also used, but the transition frequency f_T of the lateral p-n-p transistors severely limits the frequency performance of the conveyor design. An all-n-p-n implementation has also been proposed, but it shows high values of intrinsic resistance.

In our work, we propose a new CMOS CCCII with high performance, based on a CMOS compound transistors cross-coupled structure.

The Proposed Circuit

The CCCII circuit symbol is illustrated in Figure 1 and its ideal defining equation can be given as a matrix, seen in Equation 1:

$$\begin{bmatrix} I_y \\ V_x \\ I_z \end{bmatrix} = \begin{bmatrix} 0 & 0 & 0 \\ 1 & R_x & 0 \\ 0 & \pm 1 & 0 \end{bmatrix} \begin{bmatrix} V_y \\ I_x \\ V_z \end{bmatrix} \quad (1)$$

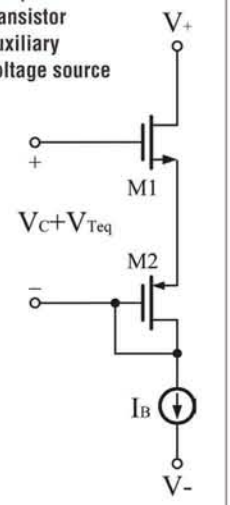

Figure 3: CMOS compound transistor auxiliary voltage source

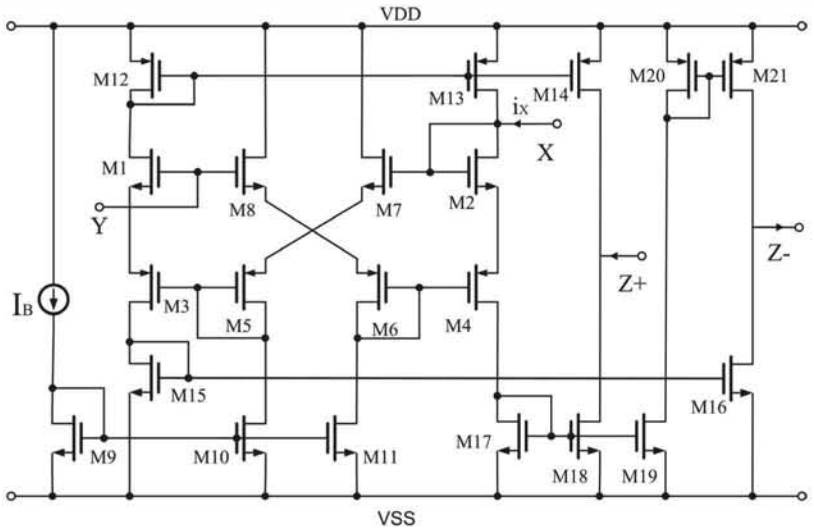

Figure 4: The proposed CMOS compound transistor cross-coupled CCCII

An improved version of an auxiliary source cross-coupled circuit is shown in Figure 2a. The N-channel differential pair and auxiliary source consisting of N-channel MOS transistors are replaced with CMOS compound transistors. The improvement makes the voltage of the auxiliary source constant, without being affected by current variations of the input differential pair, and the transfer characteristic of the differential input stage can realize ideal linear relations in a wide range.

In Figure 2a the two voltage sources V_C+V_{Teq} are cross-linked via the gates of the two CMOS compound transistors to isolate them from the drain-source circuit of the M1-M4 transistors. According to the current equation of a MOS in saturation, when the drain conducts a current, its gate-source bias voltage should be:

$$V_{GS}=\frac{1}{\sqrt{K}}\cdot\sqrt{I}+V_T \qquad (2)$$

where V_{GS} is the gate-source voltage, V_T is the threshold voltage, $K=(W/L)\mu C_{ox}/2$ is the transconductance, W and L are the width and length of the transistor channel, μ is the effective surface carrier mobility and C_{ox} is the gate oxide capacitance per unit area. The channel length modulation effect is not included in Equation 2.

When the CMOS compound transistor in Figure 2b conducts bias current, its equivalent gate-source bias voltage expression is:

$$V_{GSeq}=\frac{1}{\sqrt{K_{eq}}}\cdot\sqrt{I}+V_{Teq}$$

$$=\left(\frac{1}{\sqrt{K_n}}+\frac{1}{\sqrt{K_p}}\right)\sqrt{I}+\left(V_{Tn}+V_{Tp}\right) \qquad (3)$$

From Equation 3, the equivalent parameter of CMOS compound transistor is:

$$K_{eq}=\frac{K_nK_p}{\left(\sqrt{K_n}+\sqrt{K_p}\right)^2}$$

$$V_{Teq}=V_{Tn}+V_{Tp} \qquad (4)$$

When there's differential voltage at the input terminals, assuming the equivalent gate-source voltage of the two-CMOS-compound-transistor M1- M4 is equal to V_{GS1eq} and V_{GS2eq}, then V_{Teq} and K_{eq} of the compound transistors are equal, respectively. So, we get the following equations:

$$I_{D1}=K_{eq}\left(V_{GS1eq}-V_{Teq}\right)^2 \qquad (5)$$

$$I_{D2}=K_{eq}\left(V_{GS2eq}-V_{Teq}\right)^2 \qquad (6)$$

Taking the differences between I_{D2} and I_{D1} as input current i_X:

$$i_X=I_{D2}-I_{D1}$$

$$=K_{eq}\left(V_{GS1eq}+V_{GS2eq}-2V_{Teq}\right)\left(V_{GS2eq}-V_{GS1eq}\right) \qquad (7)$$

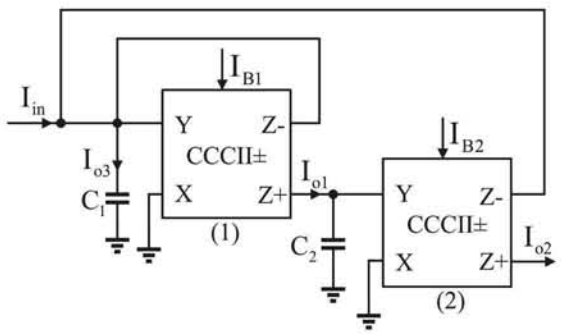

Figure 5: Electronically-tunable current-mode universal filter based CCCII

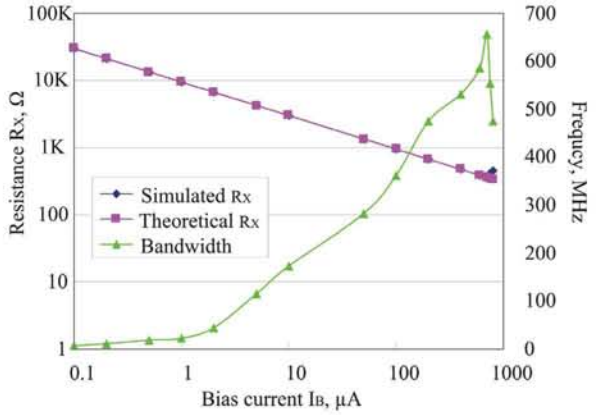

Figure 6: I_B vs transresistance and its bandwidth

From Figure 2a we get:

$$V_{GS1eq}+V_{GS2eq}-2V_{Teq}=2V_C \quad (8)$$

$$(V_{GS2eq}-V_{GS1eq})/2=V_X-V_Y=V_{XY} \quad (9)$$

From Equations 7-8 we obtain:

$$i_X=4K_{eq}V_CV_{XY} \quad (10)$$

Thus, this configuration exhibits a perfectly linear transresistance $R_X=1/(4K_{eq}V_C)$ when the auxiliary voltage source V_C is constant. The circuit implementation can be done by substituting the two floating auxiliary voltage sources.

The CMOS compound transistor auxiliary voltage source is shown in Figure 3; I_B is the bias current and the PMOS M2 transistor is connected as a diode.

The expression for the CMOS compound transistor auxiliary voltage source stems from Equation 4:

$$V_{GSeq}=V_C+V_{Teq}=\sqrt{\frac{I_B}{K_{eq}}}+V_{Teq} \quad (11)$$

$$V_C=\sqrt{\frac{I_B}{K_{eq}}}$$

V_C can be tuned by changing the value of I_B, and K_{eq} as in Equation 4.

The Proposed CMOS Compound Transistors Cross-Coupled CCCII

The complete implementation is shown in Figure 4, which takes the CMOS compound transistor auxiliary voltage source as V_C+V_{Teq} and utilizes several unity gain current mirrors.

Assuming that all FETs are enhancement-mode type, biased in saturation with substrates connected to their respective sources, the body effect can be ignored and the transistor drain current is approximated by the following relation:

$$I_D=K(V_{GS}-V_T)^2 \quad (12)$$

If the transistors have matched polarities, we can derive the following equations:

$$V_{XY}=V_X-V_Y=V_{GS2}+V_{GS4}-(V_{GS6}+V_{GS8}) \quad (13)$$

$$V_{GS2}+V_{GS4}=V_{GSeq}=\sqrt{\frac{I_{D2}}{K_{eq}}}+V_{Teq} \quad (14)$$

$$V_{GS6}+V_{GS8}=V_C+V_{Teq} \quad (15)$$

From Equations 13-15:

$$V_{XY}=\sqrt{\frac{I_{D2}}{K_{eq}}}-V_C \quad (16)$$

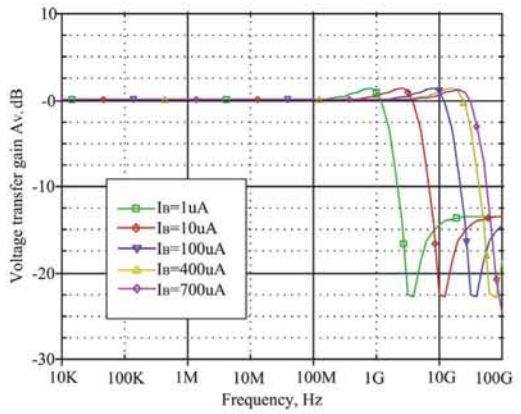

Figure 7: Voltage transfer gain at various bias currents

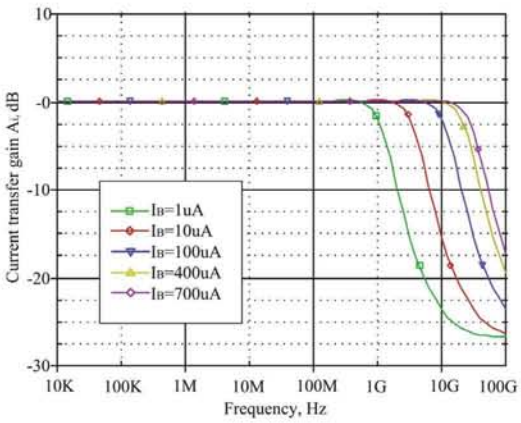

Figure 8: Current transfer gain at various bias currents

So, for the input stage circuit:

$$I_{D2}=K_{eq}\left(V_C+V_{XY}\right)^2 \tag{17}$$

From this it follows that:

$$I_{D1}=K_{eq}\left(V_C-V_{XY}\right)^2 \tag{18}$$

So the input current at the X terminal is:

$$i_X=4\sqrt{I_B K_{eq}}V_{XY} \tag{19}$$

From Equation 19, we know the transresistance gain of the CCCII is:

$$R_X=\left(4\sqrt{I_B K_{eq}}\right)^{-1} \tag{20}$$

Using 1:1 current mirrors in Figure 4, we get the following equation:

$$i_{Z+}=-i_{Z-}=i_X \tag{21}$$

When I_{D1} or I_{D2} become zero, we obtain the maximum linear input range using Equations 17 and 18:

$$-\sqrt{\frac{I_B}{K_{eq}}}\le V_{XY}\le\sqrt{\frac{I_B}{K_{eq}}} \tag{22}$$

Simple Electronically-Tunable Current-Mode Universal Filter-Based CCCII

The CCCII can be made electronically tunable for different applications. There is a new triple-output universal filter with a single input employing only four elements, as shown in Figure 5. This filter contains only two grounded capacitors and does not require any additional passive resistance. This structure can be characterized by the following expressions:

$$\frac{I_{in}-I_{o1}-I_{o2}}{SC_1}-I_{o1}R_{X1}=0 \tag{23}$$

$$\frac{I_{o1}}{SC_2}-I_{o2}R_{X2}=0 \tag{24}$$

where S is the complex frequency domain coefficient, and $R_{Xi}(i = 1, 2)$ is the intrinsic resistance of CCCII(A) and (B), respectively. Then the transfer function of this circuit is given as:

$$\frac{I_{o1}}{I_{in}}=\frac{SR_{X2}C_2}{S^2R_{X1}C_1R_{X2}C_2+SR_{X2}C_2+1} \tag{25}$$

$$\frac{I_{o2}}{I_{in}}=\frac{1}{S^2R_{X1}C_1R_{X2}C_2+SR_{X2}C_2+1} \tag{26}$$

4 Years From Now (4YFN) is an event of Mobile World Capital Barcelona and GSMA Mobile World Congress, the premier event for global mobile industry, with more than 85,000 attendees, 4500 CEOs and more than 1800 exhibitors.

For more information go to 4YFN.com

*all tickets include access to Mobile World Congress on March 5th.

An event of

MOBILE WORLD CAPITAL BARCELONA

MOBILE WORLD CONGRESS

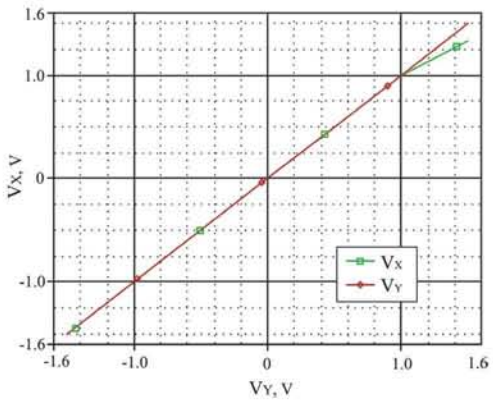

Figure 9: DC voltage transfer characteristics

$$\frac{I_{o3}}{I_{in}} = \frac{S^2R_{X1}C_1R_{X2}C_2}{S^2R_{X1}C_1R_{X2}C_2 + SR_{X2}C_2 + 1} \quad (27)$$

$$\frac{I_{o3} + I_{o2}}{I_{in}} = \frac{S^2R_{X1}C_1R_{X2}C_2 + 1}{S^2R_{X1}C_1R_{X2}C_2 + SR_{X2}C_2 + 1} \quad (28)$$

$$\frac{I_{o3} - I_{o1} + I_{o2}}{I_{in}} = \frac{S^2R_{X1}C_1R_{X2}C_2 - SR_{X2}C_2 + 1}{S^2R_{X1}C_1R_{X2}C_2 + SR_{X2}C_2 + 1} \quad (29)$$

Equations 25-29 show that the proposed filter produces bandpass, lowpass, highpass, bandreject and all-pass responses simultaneously at its outputs. The natural frequency and quality factor of the proposed circuit can be obtained as:

$$\omega_0 = \frac{1}{\sqrt{R_{X1}C_1R_{X2}C_2}} \quad (30)$$

$$Q = \sqrt{R_{X1}C_1/R_{X2}C_2} \quad (31)$$

From these equations, due to the transresistance $R_{Xi}(i = 1, 2)$ is controlled by the bias current $I_{Bi}(i = 1, 2)$, and the natural frequency ω_0 and quality factor Q can be adjusted by changing $I_{Bi}(i = 1, 2)$.

Simulation Results

PSPICE simulations based on TSMC's 0.18μm RF CMOS technology parameters are conducted on the CCCII shown in Figure 4 with ±1.5V supplies, with bias current ranging from 0.1-700μA. During the simulation, the W/L ratios of all MOSFETs are of the same scale, 1.98μm/0.18μm.

Figure 6 represents the variation of transresistance (simulated and theoretical) and its bandwidth as a function of bias current I_B; it can be seen that bandwidth increases and transresistance decreases as I_B increases between 0.1-700μA.

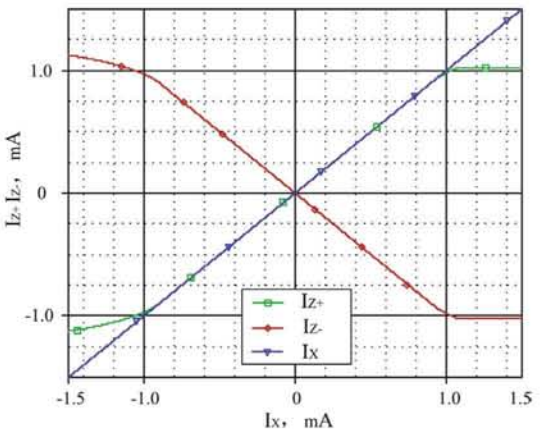

Figure 10: DC current transfer characteristics

As shown, there is a good agreement between the simulated and theoretical values of the controlled resistance.

Figures 7 and 8 show the dynamic characteristics of the voltage and current transfer gains, which confirms that the CCCII is a good performer as voltage or current follower at various bias currents, within 3dB over the bandwidth. This 3dB response of both gains tends to be greater than the transresistance's responses for the corresponding bias currents and it also displays low peaking value (< 2dB). Thus, the frequency characteristics of the proposed structure in operation

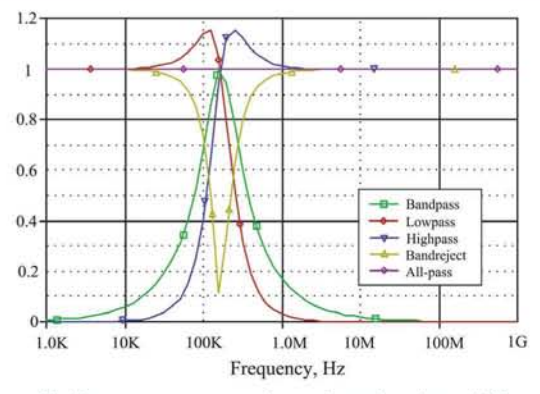

Figure 11: Frequency response of current-mode universal filter based CCCII for $I_{B1} = I_{B2} = 100\mu A$

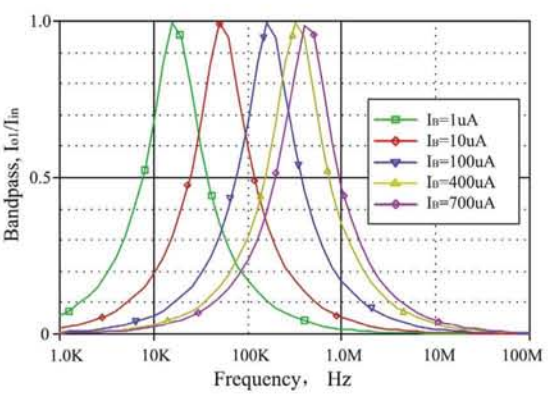

Figure 12: Bandpass responses of the filters for various $I_B = I_{B1} = I_{B2}$

FOUR INDUSTRY SECTOR EVENTS UNDER ONE ROOF

DESIGN & TEST

COMPONENTS & POWER

EMBEDDED & SOFTWARE

PRODUCTION & EMS

NATIONAL ELECTRONICS WEEK

Birmingham NEC - The Pavilion Hall
21st - 22nd April 2015

- PXI Show
- Test & Measurement Masterclass
- ECSN Technical Seminars
- Embedded Masterclass
- NPL & Smart Group Printing & Assembly Automatic Optical Inspection Experience
- Hand Soldering Competition

Book your stand space now! Call 01483 420 229

Don't miss the UK's most comprehensive electronics event

- Meet with suppliers, manufacturers and distributors
- Find out about the latest news and innovations in the industry
- Meet new companies and experience their products first hand
- Get involved in the technical content and seminar program
- Meet face to face with your contacts to secure the best business deals

Exhibitors include:

Adaptsys, amfax, ASPEN, A.T.E. SOLUTIONS, CODICO, ConRo ELECTRONICS, CoreTest technologies, COTSWORLD PLASTICS LTD, TECHNOLOGY, europlacer, HumiSeal, ELITE7, LCL ELECTRONICS, UNITEMP Environmental Test Equipment, PACE worldwide, eCosCentric, ecotile, FIPA, GOPEL electronics, O'DELL REWORK, BAE SYSTEMS INSPIRED WORK, HCD, PRE-MET, Lighthouse, FLAIR, SAMSUNG TECHWIN, LPKF Laser & Elektronika, exception, esd, TTid.co.uk, Cupio, UL, Signadyne, hitex DEVELOPMENT TOOLS, ISMsys, britton e-m-s, ART, DKL METALS LTD, ECOPAC, ROHDE&SCHWARZ, TELEDYNE LECROY, Bird Technologies, KEYSIGHT TECHNOLOGIES, NATIONAL INSTRUMENTS, JTAG TECHNOLOGIES, TE, GEYER, Medi, MAC-PANEL, pickering, PEAKGROUP, TDK·Lambda, THERMAL ISSUES, ViaSat, ZEN, APPLICOS

Find out more:

www.new-expo.co.uk/newuk

Call 01483 420 229 or email info@new-expo.co.uk

Or keep in touch by following

twitter.com/NEW_expo facebook.com/NationalElectronicsWeek linkedin.com/groups/National-Electronics-Week-2684878

Our partners and associations include:

PECM Global Success Through Innovation, ENGINEERING UPDATE, Radio-Electronics.com, emsnow, Electronics WORLD, Electronic Product Design&Test, Electronics, ecsn, SMART GROUP, VEHICLE electronics, The PXI Show, Electronics Weekly.com, COG, Electronic Specifier, The Embedded Masterclass, IET The Institution of Engineering and Technology, NPL National Physical Laboratory, smttoday, UK TRADE & INVESTMENT, Softei.com

can be assumed to be dominated by the transresistance's bandwidth, which can be referred to as CCCII's opened-loop bandwidth.

Static characteristics of the voltage and current transfers are also shown in Figures 9 and 10, confirming good linear response and with a very low offset value. From the curves in these figures, we find that the X and Y ports' voltage exhibits a linear one-to-one voltage matching characteristic over a large range, the same as the current following, validating the accuracy of Equation 1.

As shown in Table 1, performance of this proposed CCCII is verified as better, including superior linearity and input range, precise voltage and current following, low offset, large 3dB bandwidth, low noise, and so on.

The validity of the proposed filter is verified using PSPICE. For these simulations with passive components C1 = C2 = 1nF, CCCII is implemented using the model of Figure 4. The supply voltage is ±1.5V and the bias current $I_{B1}=I_{B2}= 100\mu A$. The results shown in Figure 11 validate the feasibility of the proposed circuit. Figure 12 shows the bandpass response of the filter as function of CCCII's bias current; we also can make $I_{B1} \neq I_{B2}$ to make it suitable for more applications.

CCCII	[18]	[16]	[19](*)	This work
Technology	0.8μm BiCMOS technology	AMS 0.35μm CMOS model	0.8μm BiCMOS technology	TSMC 0.18μm RF CMOS technology
Bias current	500μA	555μA	550μA	500μA
Voltage follower				
Linear input range of V_Y	-2.1V~0.25V	-0.5V~0.3V	-0.51V~0.25V	-1.49V~1.07V
Out offset at V_X	-6.0mV		-2.8mV	1.4mV
Voltage transfer gain	0.99	0.9745	0.98	1.001
-3dB bandwidth	0-4.5GHz	0-1.42GHz	0-3.2GHz	0-34.07GHz
THD(sim.)$\lvert V_Y(t)\rvert$=10mV	0.0025%		0.0015%	0.00013%
Noise at 10MHz(sim.)	5.2nV/√Hz		3.5nV/√Hz	5.3nV/√Hz
Current follower				
Linear input range of I_X	-0.5mA~0.5mA	-0.45mA~0.3mA	-0.58	-0.88mA~0.91mA
Out offset at I_Z	3μA	8.87μA	mA~5mA	-1.04μA
Current transfer gain	0.99	0.9782	-1.2μA	0.999
-3dB bandwidth	0-2GHz	0-1.39GHz	0.99	0-22.91GHz
THD(sim.)$\lvert I_X(t)\rvert$=100μA	0.05%		0-2.2GHz	0.00012%
Noise at 10MHz(sim.)	71.4pA/√Hz		0.1%	10.99pA/√Hz
			54.1pA/√Hz	
Supply voltage	±2.2V	±1.5V	±2.2V	±1.5V
Power consumption	9mW	4.864mW	14mW	12mW

(*) Simulated for n = 1

Table 1: Performance comparison with published CCCII

THE UK DEVICE DEVELOPERS' CONFERENCE ANNOUNCES DATES FOR 2015

www.device-developer-conference.co.uk

The UK Device Developers' Conference, one of the UK's leading events for engineers and scientists working to develop intelligent systems and devices, has announced dates and places for 2015. This year's the conference will be in Reading, Cambridge, Manchester and Uphall (Scotland) on the 12th and 14th May and the 2nd and 4th June respectively.

"This is a conference for those who develop electronic systems and intelligent devices," said Richard Blackburn, Conference Manager. "Engineers and software developers are very often working under pressure and to strict deadlines."

Consisting of a tools and technology vendor exhibition, two streams of hardware and software technical presentations and a series of half-day technical workshops, the UK Device Developers' Conference has become respected for its high level of technical content, providing developers with an opportunity to learn about new technologies and industry trends.

Admittance to the conference is free for developers and technical managers, and includes lunch and refreshments.

The subject of the conference this year is "*IoT in The Real World*".

"For many engineers, IoT might be considered hip media terminology," said Matt Cook, Business Development Manager at Solid State Supplies, UK provider of semiconductors and modules for embedded systems development. "IoT is not exactly an engineering term, however, machine and device connectivity is changing the world, whether it's [in the sector of] cars, medical equipment or even retail technology, its impact has been pervasive. In this presentation we will explore and compare the communication options available to engineers."

Solid States Supplies's presentation will explore options such as Wi-Fi, Bluetooth, ZigBee, Wimax, LTE and HSPA and it will evaluate each in terms of throughput, range, coverage, power consumption, devices per network, security, topology, connection and reliability. The presentation will also discuss hardware and software options, as well as solutions for device-to-cloud connectivity and security.

www.device-developer-conference.co.uk

USING GAS SENSORS IN WIRELESS ENVIRONMENTAL MONITORING AND CONTROL APPLICATIONS

IN THIS SERIES, **PROFESSOR DOGAN IBRAHIM** OF THE NEAR EAST UNIVERSITY IN CYPRUS PRESENTS DIFFERENT TYPES OF RF SYSTEMS FOR EMBEDDED APPLICATIONS. IN THIS ARTICLE, HE DISCUSSES GAS SENSORS, AND PRESENTS THE DESIGN OF A WIRELESS, MCU-BASED CARBON MONOXIDE DETECTOR

Carbon monoxide (CO) is an odourless, colourless and tasteless toxic gas. It has 200 times greater affinity with haemoglobin than oxygen, binding itself to it, preventing the blood from carrying it around the body.

Over the past century, CO levels have grown in the environment as a result of increased number of vehicles and fossil-fuel-burning appliances, including furnaces, fireplaces, grills and woodstoves, as well as gas water heaters and stoves.

Usually, there are high levels of CO in the air along main roads and in places of poor ventilation, such as tunnels, closed car-parks, garages and so on. Nowadays, most cars are equipped with catalytic converters that change the CO gas into CO2 which is not harmful to the body. Although this lowers considerably the CO produced from each vehicle, CO is still on the increase, especially in large cities.

Halth effects associated with CO are shown in Table 1.

Gas Sensors

There are many gas sensors commercially available; Table 2 lists some of the popular ones.

The operation of all gas sensors is very similar: the sensor contains a heater element, heated by external voltage – usually +5V. The sensor's load resistance is connected across the output terminals.

The surface resistance of the sensor changes when in contact with the gas to be measured. This change is detected by measuring the voltage across the load resistance. The actual gas concentration in ppm can then be calculated by making reference to the sensor's datasheet. In this article, the MQ-7 CO sensor is used; its details are given in Figure 2.

Figure 1: MQ-7 CO sensor

The MQ-7 CO Sensor

MQ-7 is a MOS sensor with a thick film of polycrystalline SnO2, which detects CO gas in the range of 20-2000ppm. When the sensor is in contact with CO or H2, a reaction takes place which decreases the surface resistance of the sensor. The basic chemical reaction inside the sensor is:

$$SnO_2 + 2CO \longrightarrow Sn + 2CO_2$$

In this reaction, when the sensor's sensitive layer made of tin dioxide (SnO2) is in touch with CO, Sn separates from the molecule and CO2 gas is released. This reaction decreases the sensor's resistance and causes a voltage to be output, an indication of the CO concentration.

MQ-7 is a 6-pin sensor (Figure 1), where only four pins are used: two for the heater, and one each for ground and power supply. The operation of the heater is different from other gas sensors. Here, the heater temperature is cyclically raised above its normal value in order to burn off impurities that may affect the reading. The heater voltage

is set periodically to +5V for 60 seconds to purge the impurities, and then to +1.4V for 90 seconds. The actual CO concentration is read at the end of the 90-second measurement period; the entire cycle takes 2.5 minutes.

It is recommended by the manufacturer that the heater is pre-heated with full power once only for a minimum of 48 hours before being used to sense CO. Afterward, the heater voltage should be set to +5V for 500 seconds before any readings are taken. The steps to make an actual CO reading are summarised below:

- Pre-heat sensor for 48 hours (once only);
- Pre-heat sensor for 500 seconds (every time power is applied);
- Apply +5V to the heater for 60 seconds;
- Apply +1.4V to the heater for 90 seconds;
- Take a CO reading;
- Repeat steps 3 to 5 as required.

Figure 2 shows the heating cycle of the sensor and the data sampling points when the sensor is exposed to CO gas. Notice that the CO gas concentration should be read at the end of the 90-second heater-low-voltage period.

The sensor surface resistance R_S when the sensor is exposed to CO is obtained by connecting a load resistance R_L across the sensor, where:

$$R_s = R_L \frac{(V_C - V_{RL})}{V_{RL}} \quad (1)$$

Thus, the surface resistance R_S at any CO concentration can be found by measuring the voltage across the load resistance. Figure 3 shows the MQ-7 response curve. Here, R_O is the sensor surface resistance when the sensor is exposed to 100ppm CO gas. Thus, by knowing the ratio R_O to R_S we can read the gas concentration in ppm from the horizontal axis. The graph in Figure 3 is described with the following equation:

$$-1.4 + \log (R_S/R_O) = -0.7 \log (ppm) \quad (2)$$

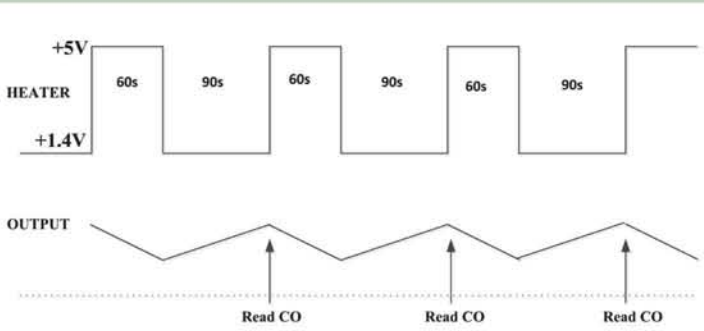

Figure 2: MQ-7 heating cycle and reading the gas concentration

Level of CO (ppm)	Health effects
0.1	Fresh air
9	Maximum recommended indoor level
10-50	Maximum exposure in workplace. Exposure for a few hours as no symptoms
100	Slight headache after 1-2 hours
200	Nausea, dizziness, headache after 2-3 hours
400	Headache and nausea after 1-2 hours. Life threatening after 3 hours
800	Headache, nausea, dizziness after 45 mins. Death within 2-3 hours
1600	Headache, nausea, dizziness after 20 mins. Death within 1-2 hours
4000	Headache, nausea, dizziness after 5 mins. Death within 30 mins

Table 1: Effects of CO poisoning and possible symptoms

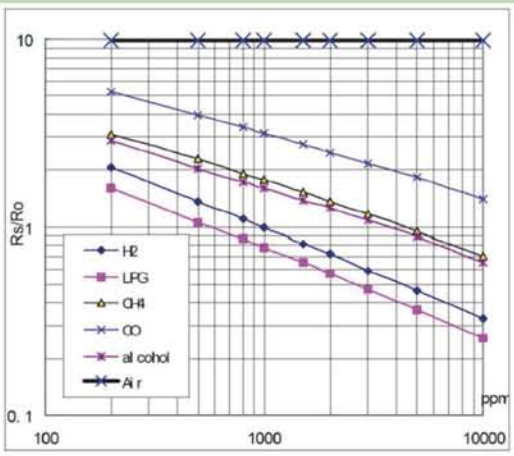

Figure 3: MQ-7 response curve

The Test System

Figure 4 shows the block diagram of the test system I developed. The transmitting side consists of the MQ-7 CO sensor chip, the Start USB for PIC development kit and a transmitting modem module. Start USB for PIC kit is a PIC-microcontroller-based development board, with the MCU operating with an 8MHz crystal.

The receiving side consists of a receiving modem module, processor (an MCU, a PC, Raspberry Pi or otherwise) and a display.

Modem Modules

Radiometrix is a UK-based developer and manufacturer of TX/RX wireless modem modules for telemetry applications, and for this project in particular, there is a large choice of modem modules, where the user can select from VHF/UHF, single-channel/multi-channel, narrowband/wideband, low-power/medium-power/high-power and transmit-only/receive-only modules.

For us, it is appropriate to choose a single-channel modem module; Table 3 gives a summary of the Radiometrix modules. Any of the serial modem modules given in this table can be used in this project.

The operation principles of these modules are all similar where the modem is connected to power and ground terminals, an antenna is connected to the modem, and the serial data pin is connected to the UART output (or input) of the microcontroller. In this project data is sent using the built-in UART module of the PIC18F2550 microcontroller.

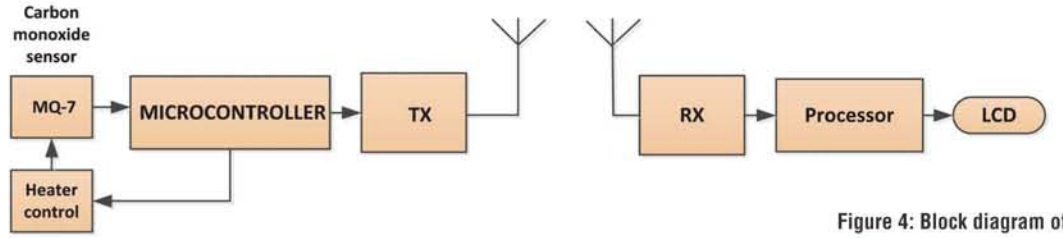

Figure 4: Block diagram of the test system

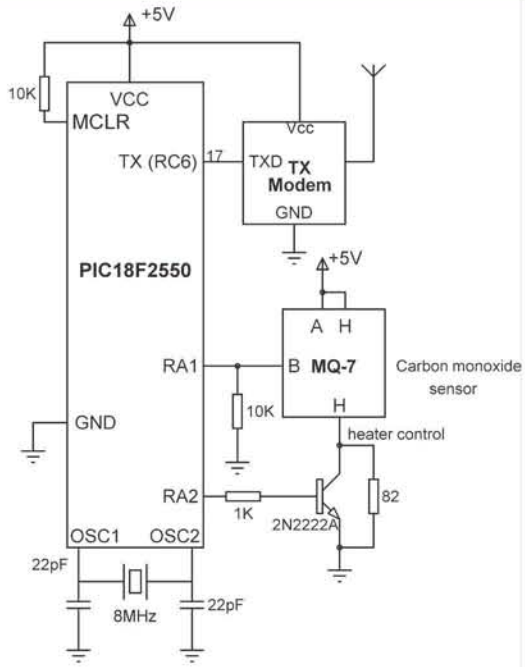

Figure 5: Circuit diagram of the transmitter

Sensor model	Used to detect
MG811	Carbon dioxide
MQ-3	Alcohol
MQ-6	LPG
MQ-7	Carbon monoxide
MQ-5	Natural gas
MQ-131	Ozone
MQ-135	Air quality
MQ-4	Methane
MQ-8	Hydrogen

Table 2: Some popular gas sensors

Figure 5 shows the circuit diagram of the transmitter. The transmitter modem module is connected to the MCU's UART output pin. The CO sensor is connected to an analog input channel 1 (RA1) of the built-in ADC converter of the PIC microcontroller through a 10K load resistor. The ADC has a resolution of 10-bits (1024 quantization levels) and operates with a +5V reference voltage. The cycling heater voltage is obtained using an NPN transistor connected to digital output RA2 of the microcontroller.

The resistance of the heater coil is 33 ohms. When the transistor is turned ON, full +5V voltage is applied to the heater coil. When the transistor is OFF, current flows through the 82-ohm resistor, producing +1.4V across the heater.

The Software

The test system's software is based on the mikroC Pro for PIC language.

Figure 6 shows operation of the transmitter program which executes in an endless loop. At the beginning of the program Timer 0 is configured to interrupt every second and timer interrupts are enabled.

Initially, full power is applied to the sensor for the first 500 seconds before any reading is taken. The code executes inside the timer interrupt service routine. Here, power to the heater is cycled with 60 seconds at +5V, and 90 seconds at +1.4V. At the end of the low cycle the CO data is read by calling function Read_MQ7(). The CO level is then calculated in ppm by calling function Calculate_ppm(), and the data is sent to the receiving station via the UART. The CO concentration is calculated with a formula.

For accurate measurements the device should be calibrated using a 100ppm pure CO source. The sensor surface resistance at this reading corresponds to R_0 and the CO concentration can be found from the graph in Figure 3, by calculating the ratio R_S/R_0. In this example R_0 is taken as 2000 ohms, which is a typical value.

Modem	Operating band	TX power	RX sensitivity	Operating voltage
RPM1	VHF	100mW	-115dBm	+3.3V or +5V
CLX2	UHF	2mW	-95dBm	+3.3V
DWA3	UHF	5mW	-106dBm	+5V
M48-169-BiM1H	VHF	500mW	-113dBm	+6V to +15V
M48-434-NiM2	UHF	10mW	-113dBm	+6V to +15V
RPM2A	UHF	10mW	-100dBm	+3V or +5V
RPM3	UHF	10mW	-100dBm	+3V or +5V
SPM2	UHF	10mW	-95dBm	+3V or +5V
TDL3F	UHF	25mW	-106dBm	+5V

Table 3: Radiometrix single-channel modem modules

```
BEGIN
        Configure microcontroller I/O ports
        Configure UART
        Turn heater on for 500 seconds
        Configure Timer 0 to interrupt every second
        Load timer registers
        Enable timer interrupts
        Wait for timer interrupt
    END

    BEGIN/TIMER INTERRUPT
        Reload timer registers
        IF 60 seconds elapsed and heater is at +5V THEN
            Turn OFF heater
        ENDIF
        IF 90 seconds elapsed and heater is at +1.4V
THEN
            Read MQ7 data
            Calculate CO ppm
            Send ppm to TX modem via UART
        ENDIF
    END/TIMER INTERRUPT
```

Figure 6: Operation of the transmitter program

```
BEGIN
        Configure I/O ports
        Configure UART
        Initialize LCD
        DO FOREVER
            Read CO ppm from RX modem via
UART
            Display data on LCD
            ENDIF
        ENDDO
    END
```

Figure 7: Operation of the receiver program

```
sbit MQ7_Data_Dir at TRISA1_bit;
sbit MQ7_Heater_Dir at TRISA2_bit;
sbit MQ7_Heater at RA2_bit;
unsigned char HeaterCycle = 0;
unsigned int seconds = 0;

float Calculate_ppm(float v)                    // Calculate ppm
{
 float Rs, ratio, p;
 float Rl = 10000.0;
 float Ro = 2000.0;
 Rs = Rl * (5-v) / v;
 ratio = Rs/Ro;
 p = 100.468/(pow(ratio, 1.43));
 return p;
}

void Read_MQ7()
{
 float Vrl, ppm;
 Vin = ADC_Read(1);                             // Read from channel 1 (CO)
 Vrl = ((float)Vin*5.0) / 1024.0;               // in volts (Vrl)
 ppm = Calculate_ppm(Vrl);                      // Calculate CO ppm value
 FloatToStr(ppm, MQ7);                          // Convert to floating point
}

void interrupt()
{
 TMR0H = 0x48;
 TMR0L = 0xD2;                                  // Reload TMR0
 seconds++;                                     // Increment seconds
 if(HeaterCycle == 0)                           // If no heater cycle
 {
 if(seconds == 500)                             // Wait for 500 seconds
 {
 seconds = 0;
 HeaterCycle = 1;
 }
 }
 else
 {
 if(seconds == 60 && MQ7_Heater == 1)           // 60 sec ON time
 {
 MQ7_Heater = 0;
 seconds = 0;
 }
 if(seconds == 90 && MQ7_Heater == 0)           // 90sec OFF time
 {
 seconds = 0;
 Read_MQ7();                                    // Read CO concentration
        UART1_Write_Text(MQ7);                  // Send data to UART
 MQ7_Heater = 1;
 }
 }
 INTCON.TMR0IF = 0;                             // Clear TMR0 interrupt flag
}

 void main()
 {
 ADCON1 = 0x0D;                                 // RA1 is analog
 MQ7_Data_Dir = 1;                              // RA1 is input (MQ7)
 MQ7_Heater_Dir = 0;                                    // RA2 is output
(heater)
 MQ7_Heater = 1;                                // Heater ON for 5000s
 UART1_Init(9600);                              // Initialize UART
 //
 // Configure TMR0
 //
 TMR0H = 0x48;                                  // Load TMR0
 TMR0L = 0xD2;
 T0CON = 0x87;                                  // Prescaler=256, timer ON
 INTCON = 0xA0;                                  // Enable TMR0 interrupts

 while(1)                                       // Wait for timer interrupts
 {
```

Figure 8: Transmitter program

4 YEARS FROM NOW

Hall 8, Fira Montjuïc
02-04 March 2015

4yfn@mobileworldcongress.com

4YFN | An event of MOBILE WORLD CAPITAL BARCELONA | GSMA MOBILE WORLD CONGRESS

Back for a second year, 4 Years From Now is an international programme presented by Mobile World Congress Barcelona and GSMA that brings together the best mobile start-ups and entrepreneurs with investors, accelerators, incubators and corporations from the mobile ecosystem.

For three days during Mobile World Congress, 4YFN will host inspiring talks, interactive workshops, cutting-edge exhibition and unique networking opportunities for 5,000+ attendees from 70 countries. 4YFN will feature:

- 150+ SPEAKERS
- 44 SESSIONS
- 40 WORKSHOPS
- 3,600 SQM OF EXHIBITION SPACE

4YFN PROGRAMME

Each day the programme will cover a different topic, lead by globally known experts in the field of entrepreneurship and innovation. Among them the following:

Monday, 02 March – Disrupted by Mobile
Designing for Touch
Context Matters
Hyper-local Services
Big Data
New Business Models
Privacy and Cybersecurity

Tuesday, 03 March – The Internet of Things
Connected Home
Quantified Self
Wearables
Rapid Prototyping
3D Printing
Product Design

Wednesday, 04 March – Digital Media
Content Strategy
Storytelling
Transmedia
New Entertainment
Alternative Education Models
Cross-Platform Perfection

SPEAKERS

The goal of 4YFN is to provide some of the most fascinating speakers in the mobile ecosystem to share their ideas on a variety of topics, including:

Mike Butcher, Editor At Large, TechCrunch
Weili Dai, President and Co-Founder, Marvell Technology Group
Dale Dougherty, Founder and Executive Chairman,Maker Media
Maelle Gavet, CEO, Ozon Holdings
Jimmy Maymann, CEO, The Huffington Post
François Moreau, CEO, Viaccess-Orca
Yossi Vardi, Chairman, 4YFN
Martin Varsavsky, CEO, FON
Be sure to check back often for updates. For complete details visit: **4yfn.com**

HOW TO PARTICIPATE

There are several different ways to participate:

ATTEND

4YFN takes place at Fira Montjuïc during Mobile World Congress and is open to all Congress attendees. Your MWC pass includes access to this three-day programme. There is a FREE shuttle to get you between Fira Gran Via and Fira Montjuïc so you can move between the two events without the expense of a taxi. For more details visit the **4yfn.com** website.

SPONSOR OR PARTNER

There are multiple opportunities to show your support of innovation and extend your presence to multiple MWC venues. Consider partnering as a Global, Track or Main Partner. More information on these sponsor and partner opportunities are available on the **4yfn.com** website.

EXHIBIT

There are a variety of exhibition packages to show your company, products or services to a highly relevant international audience. These packages offer a way to generate new contacts and build relationships with startups, investors, corporations and media. Packages offer everything from space only to enhanced solutions that include a booth and presence at MWC.

For additional information on exhibition opportunities, go to the **4yfn.com** website or send an email to: 4yfn@mobileworldcongress.com

PCIM EUROPE 2015

PCIM Europe, Nuremberg

19-21 May 2015

www.pcim-europe.com

PCIM
EUROPE

International Exhibition and Conference
for Power Electronics, Intelligent Motion,
Renewable Energy and Energy Management
Nuremberg, 19 – 21 May 2015

PCIM EUROPE 2015 – MEETING POINT FOR EXPERTS FROM INDUSTRY AND SCIENCE

From 19-21 May 2015, many international companies will present their latest products, research findings and innovations from the field of power electronics at PCIM Europe in Nuremberg. About 400 exhibitors will demonstrate their recent developments and thereby offer a unique sector overview to more than 8,000 visitors.

POWER ELECTRONICS CONFERENCE

In parallel to the PCIM exhibition, the conference will offer 29 technical sessions, giving a thorough overview of the trends and developments in the industry. Among the highlights of this year's conference are the three top-class keynotes on "*The State-of-the-Art and Future Trend of Power Semiconductor Devices*", "*Packaging and Reliability of Power Modules – Principles, Achievements and Future Challenges*" and "*Electrochemical Battery Managements and Applications*".

In addition, on the two days prior to the conference – 17-18 May 2015 – there will be nine seminars and nine tutorials, where renowned industry experts will discuss their view of the industry power electronics technologies.

At the industry forum in Hall 6, there will be technical presentations, expert discussions, project presentations and market overviews from associations, specialist media and companies. The exhibitor forum in Hall 7 will also offer some 50 presentations, focusing of the latest developments and innovations from the exhibiting companies.

FREE ENTRY TICKETS

Entry to the event is free, but a registration is necessary. Find out more on **www.pcim-europe.com/tickets**

NATIONAL ELECTRONICS WEEK

21-22 April

NEC, Birmingham

www.new-expo.co.uk/newuk

Now in its 8th year, the annual National Electronics Week exhibition will once again be based at the NEC, Birmingham, on 21st and 22nd April 2015. This year the exhibition space has expanded an additional 400 square meters, with a grown number of exhibitors and technical content, reflecting the importance of this key event. "The NEC has always worked well for us, it is in the heart of the UK, meaning that getting there is easy for everyone – whether they are coming by car or train, and even our international exhibitors and visitors can fly right to the doorstep. It's all about making it as easy as possible for everyone in the industry to access the value that this show provides," said Claire Saunders, director of the event.

Staying with their winning formula of splitting the show into four sectors, this year the following events will take place:

Components and Power

With exhibiting companies such as Wurth Electronics, TDK Lambda, Geyer Electronics and Ecopac, there will be opportunities for students to talk to those currently working in the industry and discover the latest developments.

The Electronics Component Supply Network (ESCN) will host the seminar program, including topics such as wearable technology, lighting, the Internet of Things and energy efficiency.

Design and Test

Industry leaders exhibiting in this sector include Rohde & Schwarz, Aspen Electronics, Keysight Technologies, National Instruments, JTAG, Teledyne LeCroy and more. Again, students will be able to meet with experts on the stands and even take the opportunity to start thinking about companies they may wish to apply to.

The PXI Show will be incorporated into this area with plenty of room to demonstrate the four stages of the PXI process: modules, chassis and controllers, software and system integration. Over the two days, there also will be a dedicated Test & Measurement Masterclasses from Electronics World magazine.

Embedded and Software

This area will be made up of key exhibitors, with a full seminar program from The Embedded Masterclass, involving speakers from Freescale Semiconductor.

Production and EMS

Exhibitors here include BAE Systems, Advanced Rework Technology, Europlacer, Etek-Europe and Pace Europe. The content program is as impressive as the lineup. NPL & SMART Group will provide the Printing and Assembly Automatic Optical Inspection Experience, and there will also be the National Electronics Week Hand Soldering Competition – open to all – with an adjudicating panel of IPC-accredited trainers from Advanced Rework Technology and E-Tek Technical Services. The winner will receive a high-tech prize and a trophy.

In addition to all this, there's a media centre, where the industry's leading publications will be on hand with free copies and great subscription offers.

Tickets to the exhibition including all seminars are free of charge, as is parking and Wi-Fi access. To register go to **www.new-expo.co.uk/newuk**

SCHURTER T9 NOW AVAILABLE FOR PCB MOUNTING

Schurter's T9 fuseholder style circuit breaker series is now expanded to include Model T9-818 for PCB mounting. The new model complements the existing T9 series assortment for panel mounting, providing a complete range of mounting styles equivalent to closed fuseholders.

The T9 series feature dimensions comparable to those of traditional fuse holders, and is likewise similarly designed for direct placement on circuit boards. Schurter's existing T9 series features quick-connect terminal types for front and rear snap in panel mounting, as well as thread neck mounting.

As with all PCB mounted components, assembly costs are considerably lower because fewer materials are used and wires eliminated for full automation.

www.schurter.co.uk

MEDICAL-GRADE ISOLATED DC-DC CONVERTERS EXCEED SPECIFICATIONS

The newly launched Recom REM3, REM6 and REM10 medical DC-DC converters for patient-connected applications exceed the latest IEC 60601-1 (3rd edition) specifications for 2MOPP patient protection, and are now available in the UK from Dengrove Electronic Components.

The 3W, 6W and 10W modules feature reinforced insulation for 250VAC working voltage, 5kVAC input-to-output isolation and 8mm creepage and clearance, meeting or exceeding the IEC 60601-1 requirements. In addition, ultra-low leakage current of 2µA helps designers meet the lowest limits for medical devices, such as the 0.3mA maximum specified in North American UL 60601-1.

Design-in of the modules is simplified thanks to the convenient DIP24 outline, industry-standard pin-out, wide input-voltage ranges of 2:1 or 4:1, and choice of tightly regulated output voltages from 3.3V to 24V.

www.dengrove.com

FTDI CHIP UNVEILS HIGH RESOLUTION EVE DEVICES

FTDI Chip's Embedded Video Engine (EVE) portfolio for advanced human machine interface implementation has been further strengthened with four new ICs in the FT81xQ series. The new devices support higher-maximum screen resolutions than previously possible, increasing from the 512 x 512 pixels of the company's FT800Q/801Q offering up to 800 x 600 pixels, in order to address larger displays (7-inches and above) used in point-of-sales units, information kiosks, and others.

The FT810Q has 18-bit RGB interfacing and resistive touch functionality, while the FT811Q has 18-bit RGB interfacing and is designed for capacitive touchscreen implementation (with provision for 5-point touch detection). These are complemented by the FT812Q and FT813Q for use respectively with resistive and capacitive touchscreens, each with 24-bit RGB.

Algorithm enhancements enable smoother video playback; and screen rotation through 90° is now easier to achieve.

www.ftdichip.com

PULSONIX APPOINTS MTT FOR REPRESENTATION IN SCANDINAVIA

Pulsonix, the EDA company owned by Westdev, announced the appointment of MTT Design and Verification in Sweden to sell and service its solutions in the Scandinavian region.

Introduced in 2001, Pulsonix EDA software develops high-performance schematic design capture, simulation, PCB layout and autorouting solutions. Developed by a dedicated in-house team, each release demonstrates how the fast-growing Pulsonix product is introducing key features to offer users flexible and highly compatible software that meets the demands of PCB design today.

MTT is a distributor and since 1987 it has focused on tools and equipment to simplify the design and verification of electronic products. The company is run by engineers with over 60 years of experience from designing, supporting and selling RF, EMC and microwave products.

www.pulsonix.com

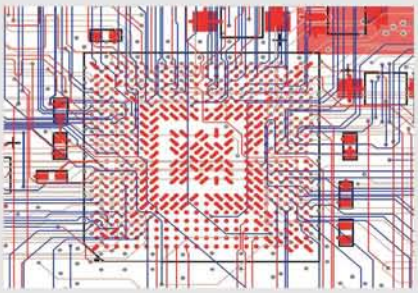

LDO FOR NOISE-SENSITIVE APPLICATIONS FROM LINEAR

The LT3042 is a leading-edge, ultralow noise, ultrahigh power supply ripple rejection (PSRR) low dropout voltage linear regulator. Its unique design features ultralow spot noise of only 2nV/√Hz at 10kHz and 0.8µVRMS integrated output noise across a wide 10Hz-100kHz bandwidth. Low and high frequency PSRR performance are exceptional.

The device's wide input and output voltage ranges, high bandwidth, high PSRR and ultralow noise performance make it ideal for powering noise-sensitive applications such as PLLs/VCOs/mixers/LNAs, very low noise instrumentation, high-speed/high-precision data converters, medical applications such as imaging and diagnostics, precision power supplies and as a post regulator for switching supplies.

The LT3042 is available in thermally enhanced 10-lead 3mm x 3mm DFN and 10-lead MSOP packages, both with a compact footprint. The E- and I-grade versions are available from stock with an operating junction temperature of -40°C to 125°C.

www.linear.com

SINGLE-OUTPUT 5-20W MEDICALLY-APPROVED POWER SUPPLIES

Powersolve has announced the PME05, PME10, PME15 and PME20 series of single output power supplies designed to provide up to 20W for medical equipment applications. Each PME series comprises four models all featuring Class II isolation, a rugged plastic housing and, importantly for medical applications, cooling by free air convection. Every model has been burn-in tested at full load.

DC output voltages for each series are 5, 12, 15 or 24V from a universal 85-264VAC input, across the operating temperature range of -20°C to +70°C. These power supplies have a no-load power consumption of less than 0.5W which will satisfy the increasing number of "green" applications.

All models are approved to EN61000-4-2, 3, 4, 5, 6, 8, 11, EN60601-1-2: 2001+1: 2006 Life Supporting Equipment, making them suitable for use in any medical systems application.

www.powersolve.co.uk

PANASONIC LAUNCHES NEW THERMOPILE ARRAY SENSOR

Panasonic Automotive & Industrial Systems has launched the first-ever surface mount thermopile array sensor. Grid-EYE features 64 thermopile elements in an 8 x 8 grid format that detect absolute temperatures by infrared radiation. Grid-EYE is able to measure actual temperature and temperature gradients, providing thermal images. It is easily possible to detect multiple persons, identify positions and direction of movement, almost independent of ambient light conditions without disturbing privacy as with conventional cameras.

Cost-effective and compact solutions for contactless temperature measurement across the entire specified area can be with very accurate results. The built-in silicon lens provides a viewing angle of 60°. The measurement values can be read out via I²C interface in 1 or 10 frames per second. The interrupt signal output delivers a quick response to time-critical events.

http://eu.industrial.panasonic.com

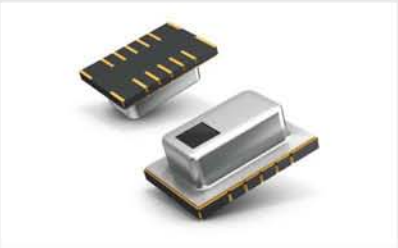

PACKAGE OF EFFECTIVE SURFACE-MOUNT EMI/RFI SOLUTIONS

Harwin has launched a package of surface mount products that can be used separately or in combination to deliver an effective EMI/RFI solution. All these products – contained within Harwin's popular EZ-BoardWare range – are designed to take advantage of surface mount technology, simplifying and speeding manufacture, reducing costs and increasing quality.

EZ-BoardWare Shield Cans are simply pressed onto pre-positioned surface-mount EZ-Shield Clips forming a Faraday cage around sensitive ICs and electronic circuitry, saving on expensive, labour-intensive secondary assembly.

Attenuation performance up to 24dB can be achieved, depending on frequency and configuration. The cans have a simple, five-sided box design, which is mechanically robust and more cost-effective than fence and cover types.

www.harwin.co.uk

ASTUTE LAUNCHES AIRBORN HIGH-DENSITY INTERCONNECT SYSTEM

Astute Electronics has introduced AirBorn's high-density, high-reliability HD4 interconnect technology, designed to be an electrically-optimized and highly dense physical-layer medium for the HyperTransport Technology Consortium's industry-standard HyperShare scalable interconnect technology. Claimed to be the smallest footprint in the industry, HD4's high bandwidth, minimized signal-loss and mission-critical reliability suit it for demanding, multi-dimensional network fabrics and ultra-fast storage/SSD cluster applications used in next-generation data centre and cloud computing platforms.

Although developed for the HyperShare platform, HD4 products suit many other popular high-performance interconnect standards. The I/O link targets rack-in-cabinet-based systems that require higher bandwidth and density, providing up to six I/O ports on a 7.4mm pitch along a low-profile PCIe.

www.astute.co.uk

ROBUST, LOW-COST TX/RX FAMILY FROM OMC

OMC launched its H19 range of low-cost optical transmitter/receiver devices for polymer and large-core glass fibre systems, featuring a precision-machined metal ferrule which provides enhanced reliability for industrial applications. The range includes both single-channel devices, for use with simplex fibre, and dual-channel devices, with duplex connectors facilitating transceiver operation.

Most connector systems for use with polymer fibre are produced almost entirely out of plastic, including the ferrule that attaches to the fibre. This provides a lower cost solution over metal connector systems, but can lead to reduced robustness and resilience when used in long-term industrial applications or other demanding environments.

OMC's H19 package benefits from the cost advantages of a high quality plastic housing, but with a precision-machined metal ferrule it provides a much higher level of precision.

www.omc-uk.com

NEW APPLICATION NOTE ON DESIGNING WITH GAN TRANSISTORS

GaN Systems has released a new application note for design engineers, which sets out thermal design guidelines and PCB layout choices for its enhancement-mode power switching transistors supplied in its proprietary GaNPX device packaging.

These are the first discrete power devices to be embedded in a laminate construction – conventional packaging techniques, such as clips, wire bonds and moulding compounds have been replaced with galvanic processes. These advanced design features of GaNPX packaging significantly increase the current carrying capability of GaN Systems' devices and significantly reduce critical loop inductance, making driving the high-speed, high-current switches a lot easier.

The application note gives a thermal analysis of GaN Systems's GS66508P E-mode GaN, 34A, 41mΩ power switch, together with diagrams showing its thermal dissipation paths and further explanation of how heat is dissipated by the GaNPX packaging design.

www.gansystems.com

MOUSER SIGNS GLOBAL DISTRIBUTION DEAL WITH DIGILENT

Mouser Electronics announced a distribution agreement with Digilent, a subsidiary of National Instruments. Digilent is an engineering design company serving students, universities, engineers and OEM's worldwide with technology-based educational tools.

Some of the newest Digilent products available from Mouser Electronics include the Digilent Analog Discovery USB oscilloscope and Digilent ZYBO Zynq-7000 development board. The oscilloscope is a multi-function measurement tool that turns any PC into a powerful engineering test device. It is driven by the free WaveForms software, and allows the test of analog and digital circuits in virtually any environment.

The Digilent ZYBO board features rich, ready-to-use, entry-level embedded software and digital circuit development platform. It provides an alternative to designers that wish to leverage the massive processing power and extensibility of the Zynq AP SoC architecture.

www.mouser.com

MOUSER ELECTRONICS

RUGGED DIN 41612 CONNECTORS OFFER SPACE-SAVING BENEFITS

Harting is now offering its established DIN 41612 male connectors in Type 3Q and 3R shell styles to provide space-saving benefits in applications involving high-density circuit boards using smaller components.

The density of the electronics on modern PCBs is steadily increasing, while both circuit boards and components are becoming smaller. This trend is driving the need to use smaller connectors, and so all male Harting connectors are now available with or without flanges. The male connectors without flanges offer particular space-saving benefits – although they are just as robust as existing devices in the full and half sizes.

The new male connectors in styles 3Q and 3R are particularly suited to use in mezzanine and cable to circuit-board applications, along with type 3B and 3C female connectors.

www.harting.co.uk

EASY-INTEGRATION SENSORLESS BRUSHLESS DC MOTOR CONTROLLER

The A4963 from Allegro MicroSystems Europe is a new 3-phase sensorless brushless DC motor controller IC that can be easily customised for integration into users' applications.

The new device is designed for use with external complementary p-channel and n-channel power MOSFETs. Reliable sensorless startup and run commutation can be quickly customised for individual motors and loads by adjusting a few simple default parameters, with considerable saving of design time. It can be used as a standalone controller communicating directly with an electronic control unit or in a close-coupled system with a local microcontroller.

The A4963 fits a wide range of applications since its output current requirements can be scaled up or down with external MOSFET selection. It also has a wide DC supply voltage range of 4.2-50V.

www.allegromicro.com

INDUSTRY'S FIRST MONOLITHIC EDLC CELL BALANCING IC

Rohm has recently announced the development of a cell balancing IC that contributes to increased miniaturization, greater stability and longer life for EDLCs (Electric Double Layer Capacitors), which are driving the adoption of energy regeneration applications in industrial equipment, automotive idling stop systems and voltage sag (instantaneous voltage drop) counter-measures.

The BD14000EFV-C integrates over 20 discrete components required for EDLC cell balancing on a single chip, reducing mounting area by 38% over conventional solutions while eliminating component variations, making it easy to configure compact, high-reliability EDLC systems.

In addition to cell balancing functionality for up to six cells, multiple ICs can be connected in series to enable simultaneous control of even more cells. The cell balancing voltage can be set between 2.4V and 3.1V, ensuring support for a variety of EDLCs.

www.rohm.com/eu

CUSTOM CELL PACKS POWER AIR QUALITY MONITORS

Cell Pack Solutions, specialist custom battery pack manufacturer, has designed and manufactured custom cell packs to power a new range of remote air quality and environmental measurement monitors made by Envirowatch.

Air and noise pollution and their effects on health is an increasingly serious problem, so there is a need to monitor air quality and noise pollution in a wide variety of locations.

The Envirowatch wireless sensor devices, called E-MOTES, are capable of delivering real-time air quality, noise, climate and traffic data. They are of compact design, unobtrusive and can be installed in remote and generally inaccessible locations. Data is sent every minute by wireless communication to EnviroView software that provides accurate graphical information mapped to each sensor location using GPRS sent to users' devices, enabling analysis without the need to collect data manually.

www.cellpacksolutions.co.uk

BULGIN EXTENDS BUCCANEER SMB ANTENNA RANGE

Bulgin – an Elektron Technology connectivity brand – has launched an environmentally-sealed 90° SMB antenna, offering greater flexibility in systems design for RF monitoring and control. Complementing the existing IP68-rated SMB antenna, this new option is available to suit a variety of frequency bands – from 2.4GHz and 440-470MHz to 900/1,800/1,900MHz – and can be combined with the PX0414 SMB Buccaneer panel mounting connector to provide a completely waterproof and dustproof option for RF equipment.

The Buccaneer SMB series of waterproof antennae has been developed to offer robust, hassle-free operation for industrial, scientific and medical instrumentation, as well as smart meters, base stations and outdoor hotspot installations for wireless LAN, GSM and Bluetooth. This new option promises to simplify instrument design, for straightforward installation and reliable operation in any application.

www.bulgin.com

bulgin
a brand of Elektron Technology

CABLE ASSEMBLIES FROM DC TO 50GHZ FROM INTELLICONNECT

Intelliconnect (Europe) Ltd, the UK-based specialist manufacturer of RF connectors, continues to expand its cable assembly service. Having seen considerable business growth since its launch 18 months ago, the operation is relocating to a new facility in Corby and having additional production equipment.

Intelliconnect provides high quality, UK manufactured, bespoke cable assemblies for high volume as well as specialist small batch requirements for RF applications, test and measurement and defence applications.

All types of cable assemblies are undertaken from wiring loom assemblies to high performance low-loss cables operating up to 50GHz. Coaxial, triaxial and multi-way connectors may be specified and fully immersible waterproof versions are available. All Intelliconnect cable assemblies are 100% electrically tested before despatch, and phase matching is also available.

www.intelliconnect.co.uk

CAD CONNECTED

PROTEUS DESIGN SUITE VERSION 8

Featuring a brand new application framework, common parts database, live netlist and 3D visualisation, a built in debugging environment and a WYSIWYG Bill of Materials module, Proteus 8 is our most integrated and easy to use design system ever. Other features include:

- . Hardware Accelerated Performance.
- . Unique Thru-View™ Board Transparency.
- . BSDL and PADS ASCII library part import tools.
- . Integrated Shape Based Auto-router.
- . Flexible Design Rule Management.
- . Polygonal and Split Power Plane Support.
- . Automatic support for teardrop placement.
- . Direct CADCAM, ODB++, IDF & PDF Output.
- . Integrated 3D Viewer with 3DS and DXF export.
- . Mixed Mode SPICE Simulation Engine.
- . Co-Simulation of PIC, AVR, 8051 and ARM MCUs.
- . Direct Technical Support at no additional cost.

Version 8.3 will include support for MCAD data exchange via the STEP/IGES file formats

www.labcenter.com

Labcenter Electronics Ltd
53-55 Main Street, Grassington, North Yorks, BD23 5AA
Tel: +44 (0)1756 753440 Fax +44 (0)1756 752857 Email: info@labcenter.com

Labcenter Electronics www.labcenter.com

Power Supply Analysis

Power Supply Gain - Phase

Power Supply Output Impedance

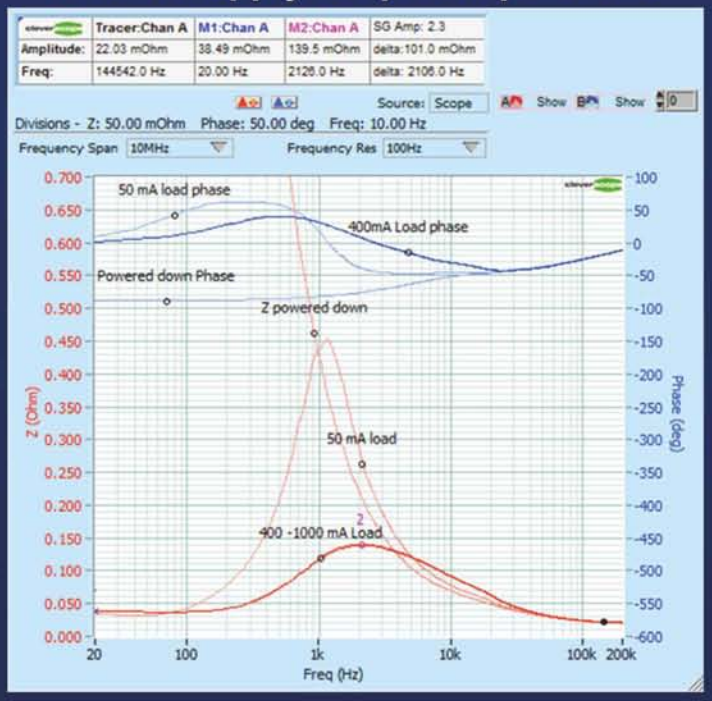

Power Supply Input Impedance

Power Supply Rejection Ratio

Use a Cleverscope CS328A-XSi to prove your Power Supply design is fit for purpose:

- Phase Margin is 50-60 degree for optimum stability and transient response.
- Gain Margin is >10dB to compensate for component and temperature variation.
- Output Impedance is low enough over frequency range to guarantee maximum voltage ripple
- Negative Input Impedance will not be unstable with input filters
- Power Supply Rejection Ratio is compatible with expected input supply disturbances.

CS328A-XSi

- Frequency Response Analyser
- 0.1Hz - 65 MHz frequency range
- >100 dB dynamic performance
- 20mV - 40V DC full scale, offset over ± 24V DC range
- 300V rms isolated signal generator

cleverscope.com/fra